Highlights

1. Poly(3-hydroxybutyrate)/hydroxyapatite scaffolds for bone tissue engineering
2. The innovative two-step fabrication procedure is proposed
3. Thermally induced phase separation was employed to obtain porous structure
4. *In situ* synthesis of hydroxyapatite was used to obtain composite scaffold
5. PHB/HA porous scaffolds can promote cells differentiation towards osteoblasts

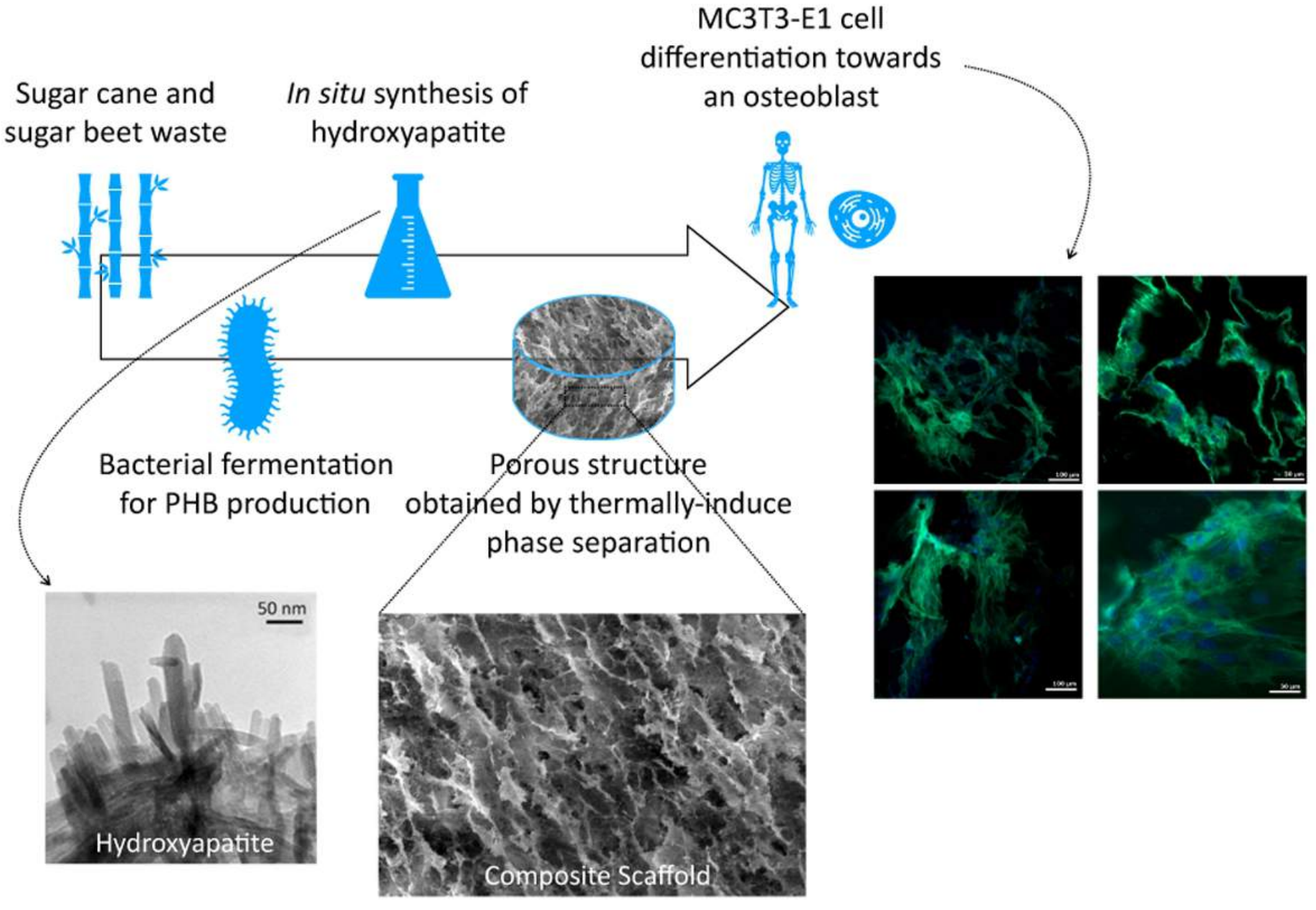
Sugar cane and sugar beet waste
In situ synthesis of hydroxyapatite
MC3T3-E1 cell differentiation towards an osteoblast
Bacterial fermentation for PHB production
Porous structure obtained by thermally-induce phase separation
50 nm
Hydroxyapatite
Composite Scaffold

Highly porous PHB-based bioactive scaffolds for bone tissue engineering by *in situ* synthesis of hydroxyapatite

Micaela Degli Esposti [a,b,*], Federica Chiellini [c,b], Federica Bondioli [d,b], Davide Morselli [a,e,*], Paola Fabbri [a,b]

[a] *Department of Civil, Chemical, Environmental and Materials Engineering, Università di Bologna, Via Terracini 28, 40131 Bologna, Italy*

[b] *Consorzio Interuniversitario di Scienza e Tecnologia dei Materiali (INSTM), Via Giusti 9, 50121 Firenze, Italy*

[c] *BIOLab Research Group, Department of Chemistry and Industrial Chemistry, Università di Pisa, via Moruzzi 13, 56124 Pisa, Italy*

[d] *Department of Applied Science and Technology, Politecnico di Torino, Corso Duca degli Abruzzi 24, 10129 Torino, Italy*

[e] *Smart Materials, Istituto Italiano di Tecnologia, Via Morego 30, 16163 Genova, Italy*

* Corresponding Authors:

Micaela Degli Esposti, micaela.degliesposti@unibo.it

Davide Morselli, davide.morselli6@unibo.it

Abstract

In this study bioactive and bioresorbable porous scaffolds for bone tissue regeneration, based on poly(3-hydroxybutyrate) (PHB), are presented. The porous structure is obtained by thermally induced phase separation (TIPS) technique, whereas the osteoinductivity and osteoconductivity are enhanced through the incorporation of hydroxyapatite (HA). The HA particles are generated in PHB using an innovative filler *in situ* synthesis, and the properties of the composite scaffolds are then compared to scaffolds obtained by conventional mechanical dispersion of *ex situ* synthesized HA particles. The *in situ* synthesis leads to composite materials with improved porosity, even at high filler content, without any degradation of the polymeric matrix as confirmed by GPC and DSC measurements. On the contrary, the samples prepared by *ex situ* method show a suppressed porosity by increasing the inorganic filler content, therefore limiting the amount of HA that can be loaded in PHB and the resulting bioactivity. The possibility to use PHB/HA porous composites as scaffolds for bone tissue regeneration, is assessed by preliminary cell viability *in vitro* studies. In particular, it is observed that the composites are fully cytocompatible and able to sustain MC3T3-E1 mouse pre-osteoblast cells adhesion and proliferation. Investigations on cell morphology reveal, for all PHB/HA scaffolds, the presence of differentiated cells with a predominance of osteocyte-like morphology, which are not observed for neat PHB scaffolds. Moreover, the MC3T3-E1 cells differentiation towards osteoblastic phenotype is further supported by the evaluation of the early osteogenic markers. In particular, samples loaded with HA *in situ* synthesized showed the highest ALP production and typical morphology of the terminal differentiation stages of osteoblasts.

Keywords: poly(3-hydroxyalkanoate)s; poly(3-hydroxybutyrate); hydroxyapatite; *in situ* synthesis; scaffolds; bone tissue engineering

1. Introduction

In the last decade, the field of scaffolds for bone tissue regeneration has been attracting great attention due to the rapid increase of musculoskeletal pathologies caused by the prolonged life expectancy.[1] For this reason several materials have been developed for inducing the tissues regeneration, where the active support is biologically degradable and replaceable by the growing cells. The most suitable approach in order to enhance the cells growth, adhesion and avoid the implant rejection is to provide to the growing cells a material with both suitable structure and chemical-physical properties.[2, 3] The porosity that mimics the bone architecture is a key factors for designing scaffolds for bone tissue engineering.[4, 5] On the other hand, it is known that the incorporation of hydryapatite (HA) in the scaffold confers high bioactivity and hydrophilicity to the system, which further promote osteogenesis and osteoinductivity.[6-8] The scaffold resorbability is another fundamental aspect that has to be considered during the material design [9] in order to avoid either to have permanent embedded implant in the patient's body or the need of an extra surgery to remove it, which are common disadvantages when metallic or ceramic material are used. According to the need to have a bioresorbable scaffold that does not release toxic degradation products, which can cause inflammations to the surrounding tissues, poly(hydroxyalkanoate)s (PHAs) completely fulfil this requirement.[10] PHAs are linear polyesters characterized by thermoplastic behaviour.[11] They are produced through a controlled fermentation process of sugar beets and sugar canes agro-wastes.[12, 13] Over hundred different types of PHAs consisting of various monomers have been reported.[14] Among them, the poly(3-hydroxybutyrate) (PHB) is indeed the most known and studied nowadays. The high biodegradability and biocompatibility of such biopolymer are not the only peculiar properties, in fact it has been recently reported that the substances released by the biodegradation of PHB can be easily metabolized by the organism.[10, 15, 16] Therefore, the combination of PHB and HA to obtain bioactive composite scaffolds represents a very interesting and valuable alternative to the usually employed ceramic or metallic materials. In fact, PHB/HA composite can promote the cell growth on a substrate very similar to the biological one with the simultaneous replacement of the biopolymeric matrix with living tissues.[17]

Concerning HA, it is known that a content between 1 and 10 wt.% offers a good balance between a favourable environment for the cells growth and adhesion and suitable mechanical properties of the scaffold.[18] The use of a nanofiller moves this range toward lower filler content (typically 1 to 5 wt.%) thanks to the high surface

area offered by the nano sizes, which lead to an extra-enhancement of the desired properties with a significantly lower filler content.[17, 19] The particles dispersion in the polymeric matrix is the most important parameter that has to be controlled in order to obtain homogeneous nanocomposite materials. Nevertheless, this is still one of the main problems of the composites preparation when mechanical and/or ultrasound mixing methods are used. It is well-known that particles obtained by flame pyrolysis or colloidal synthesis cannot be easily redispersed in polymeric matrices only using conventional mixing methods, due to their strong tendency to form micrometric aggregates.[20] An alternative method has been recently proposed by Wan et al. It is based on HA precipitation on preformed bacterial cellulose fibres immersed in the reactive solution.[21, 22] Despite such method is very interesting to obtain fibrous polymeric structure fully decorated with exposed inorganic particles, some limitations in terms of adhesion between the two materials and durability could arise. Moreover, using this approach only particles on the polymer surface are formed thus preventing the typical improvements of the mechanical and thermal properties that are observed when a rigid filler in embedded in the polymer bulk.[23] In order to overcome these drawbacks, an efficient alternative is represented by the so-called "*in situ* synthesis" of nanoparticles (NPs), where the fillers are directly synthesized in the hosting polymeric matrix, thus preventing the particles aggregation and improving their dispersion.[20] Such method has several further advantages such as it avoids the particles surface functionalization, necessary to improve the filler/matrix compatibility, when *ex situ* prepared particles are added. Furthermore, it avoids free NPs handling and the use of expensive pre-formed NPs, making this synthetic approach based on cost-effective salt precursors, particularly appreciable also from an industrial point of view. Regardless such advantages, the *in situ* formation of inorganic filler in polymers has been barely reported in literature for zero-valent metal [24, 25] and semiconductors.[23, 26, 27] Hence, further investigations are needed in order to make this synthetic strategy widely employed. The *in situ* synthesis of HA by aqueous sol-gel process in presence of PHB in the reactive solution appears to be the most promising strategy to prepare homogeneous composites thanks to the typical mild conditions of the sol-gel chemistry, which preserve the polymer from the degradation.[28] Moreover, such synthetic technique is particularly compatible with the thermally induced phase separation (TIPS) technique that is a very efficient procedure for inducing the formation of porous structures.[29, 30] Several sol–gel pathways that start from different calcium and phosphorous precursors have been proposed for the preparation of HA particles.[31] Among them,

aqueous-based routes have demonstrated to be the most suitable, mainly thanks to the fine control on Ca/P stoichiometry ratio that ensures a composition very similar to that of the bone tissues.[18, 32]

Herein we present a very innovative two-step process based on the combination of *in situ* synthesis of HA NPs in PHB solution and TIPS technique to obtain fully biocompatible and bioresorbable nanostructured composite porous scaffolds. Chemical and physical properties of the so-prepared materials were then compared with composites obtained by mechanical redispersion of HA *ex situ* synthesized in PHB solution. Then, the abilities to sustain cell viability and differentiation, of the composite scaffolds obtained by the two procedures, were investigated by using mouse calvaria pre-osteoblast MC3T3-E1 cell line.

2. Experimental

2.1 Materials

1,2-cyclohexane dicarboxylic acid diisononyl ester (Hexamoll DINCH®, DINCH) kindly supplied by BASF and calcium nitrate tetrahydrate (≥ 99.0%, $Ca(NO_3)_2 \cdot 4H_2O$) and ammonium dihydrogen phosphate (≥ 99.0%, $NH_4H_2PO_4$) supplied by Carlo Erba Reagents were used as received without further purification. Methanol (MeOH, ≥ 99.8%), ethanol (EtOH, 99.8%), 1,4-dioxane (DIOX, ≥ 99.0%), chloroform ($CHCl_3$, HPLC grade), celite (Standard Super Cel® fine) and ammonium hydroxide aqueous solution (NH_4OH, 28.0-30.0%) all from Sigma-Aldrich were used as received without further purification.

Bacterial poly(3-hydroxybutyrate) (PHB) was kindly provided by Bio-on SpA (Bologna, Italy) as experimental grade powder, which was carefully purified in order to remove all possible impurities (procedure reported in section 2.2) before the scaffold fabrication.

2.2 PHB purification

The as-received PHB was dissolved in chloroform (0.04 $g \cdot mL^{-1}$) by heating under reflux and magnetic stirring for one hour. The mixture was then filtered through a pad of celite over a sintered disk filter funnel (porosity P2) and the filtrate was precipitated in a large excess of cold methanol. Purified PHB was recovered as a white solid by filtration over sintered disk filter funnel (porosity P4) and dried at 85°C for 2 hours.

2.3 Samples Preparation

2.3.1 HA Synthesis. The sol-gel route employed to synthesize crystalline HA was optimized adjusting the procedure proposed elsewhere [18, 32] and using as precursors $Ca(NO_3)_2 \cdot 4H_2O$ and $NH_4H_2PO_4$. In particular, in a three neck round bottom flask equipped with mechanical stirring, $Ca(NO_3)_2 \cdot 4H_2O$ was dissolved in DIOX (0.259 M, solution A) by heating at 100°C under reflux until complete dissolution. An aqueous solution of $NH_4H_2PO_4$ (0.156 M, solution B) was prepared and added dropwise to solution A in approximately 1 h by using an addition funnel. Further vigorous stirring was maintained for 2 h under reflux and pH was periodically monitored and adjusted to 9 by addition of few drops of NH_4OH_{aq} (28.0-30.0%). An homogeneous dispersion was obtained by mechanical stirring and sonicating the mixtures for 1 h under reflux using the ultrasonic processor UP50H (Hielsher, 50 watts, 30 kHz), equipped with the sonotrode MS2 (titanium tip, diameter 2 mm). The formed HA was recovered as a white solid by filtration and washed twice with fresh DIOX and dried under vacuum at 80°C overnight.

2.3.2 Scaffolds Preparation Procedure. PHB/HA composites, with 2%, 5%, 8% and 10% of HA content, were prepared by using two procedures in order to have a correlation between the final properties of the material and used preparation method. In both cases, purified PHB was previously plasticized with 30 wt.% of DINCH with respect to the polymer in order to obtain suitable mechanical properties for the proposed application.

The first approach is based on the *in situ* synthesis of HA using the aforementioned sol-gel approach (described in section 2.3.1), but in presence of PHB dissolved in the reactive solution. This approach not only limits the particle aggregation, but also improves their dispersion even when the filler content is high. A typical preparation procedure was as follows: in a three neck round bottom flask equipped with mechanical stirring, purified and plasticized PHB was dissolved in 30 mL of DIOX by heating (100°C) under reflux. When PHB was completely dissolved, a given amount of solution A was added. After 30 minutes solution B was slowly added dropwise to the polymer solution over a period of approximately 1 hour. Vigorous stirring was maintained for 2 h under reflux and pH was periodically monitored and adjusted to 9 by addition of NH_4OH_{aq}. A homogeneous dispersion was obtained by stirring and sonicating the mixtures for 1 h under reflux using the ultrasonic

processor UP50H, equipped with the sonotrode MS2 (50 watts, 30 kHz). All details about the formulations are reported in Table 1.

The second method is based on mechanical/ultrasound mixing of HA *ex situ* synthesized (using the procedure described in section 2.3.1) in a PHB DIOX solution. Typically, nanocomposites were prepared by dissolving purified and plasticized PHB in DIOX by heating under reflux until complete dissolution. Then, a given amount of pre-synthesized HA was dispersed by mechanical mixing for 3 h and later by ultrasound mixing using the ultrasonic processor UP50H, equipped with the sonotrode MS2 (50 watts, 30 kHz) for 1 h (see Table 1 for more detailed information).

For comparison reasons, also neat purified PHB scaffolds were prepared by dissolving in DIOX purified and plasticized PHB by heating under reflux. The same mixing conditions used for the *in situ* and *ex situ* scaffolds preparation were also employed in order to have the same effect on the molecular weight of the polymer matrix (see Table 1 for details).

The desired porous structure was achieved using TIPS technique. Specifically, after the mixing step all the aforementioned mixtures were cast into disposable aluminum dishes (diameter 55 mm) and cooled at −18°C in a freezer. After 18 h, the frozen samples were extracted from the holders and fully immersed in EtOH bath precooled at −18°C for 72 h, with solvent refreshed every 24 h in order to remove completely the DIOX. At the end of the extraction procedure, the porous scaffolds were taken out of the freezer and carefully dried under vacuum. Five circular samples (approximately 1.1 g, diameter 55 mm and thickness 10.0 mm) per composition were prepared (representative photographs are reported in Figure S1 of supporting information).

The prepared scaffolds were coded as ES_XXXX an IS_XXXX corresponding to the procedure used for the HA synthesis. The number, which follows ES and IS, indicates the composition in weight percentage of PHB and HA in the composites.

Table 1. Formulations of the prepared samples to prepare one scaffold.

Sample	PHB/HA ratio (%/%wt.)	PHB (g)	HA (g)	DINCH content (g) *	DIOX (mL)	Solution A (mL)	Solution B (mL)
PHB	100:0	1.200	-	0.360	30.0	-	-
ES_9802	98:02	1.176	0.024	0.353	30.0	-	-
ES_9505	95:05	1.140	0.060	0.342	30.0	-	-
ES_9208	92:08	1.104	0.096	0.331	30.0	-	-
ES_9010	90:10	1.080	0.120	0.324	30.0	-	-
IS_9802	98:02	1.176	0.024	0.353	29.1	0.92	0.91
IS_9505	95:05	1.140	0.060	0.342	27.7	2.31	2.29
IS_9208	92:08	1.104	0.096	0.331	26.3	3.70	3.68
IS_9010	90:10	1.080	0.120	0.324	25.4	4.61	4.57

(*) DINCH contents were calculated as 30 wt.% with respect to the PHB amount.

2.4 Characterization

Morphology and porosity were investigated using a scanning electron microscope Nova NanoSEM (FEI) on the cross-section of the scaffolds, applying 15 KeV. HA particle distribution was observed using back-scattered electrons on dedicated samples. In detail they were prepared by drop casting, onto a silicon wafer, of a solution (20 µL) obtained dissolving 20 mg of a given scaffold in 1 mL of $CHCl_3$. The silicon wafer was then pasted on a SEM stub by using a carbon tape. Previously the investigation, the specimens were coated with 10 nm of gold. The average pore size of the scaffolds was estimated by analysing SEM images with FIJI/ImageJ open-source software.

Morphology and dimensions of the HA primary particles were investigated by a JEOL JEM 2010 transmission electron microscopy (TEM) equipped with a tungsten thermionic electron source, operating at 120 kV. About 0.005 g of HA were dispersed in 2 mL of EtOH by magnetic stirring for 1 hour. 5 µL of the so-obtained suspension were then dropped on a copper grid (300 Mesh Cu Carbon only) followed by drying at room temperature. Energy-dispersive X-ray spectroscopy (EDS, INCA 100, Oxford) was used for determine the atomic

particle composition. In order to evaluate the particles size distributions, the TEM images were analysed and processed (about 50 NPs were measured) by FIJI/ImageJ open-source.

Compression tests were carried out by a DMA Q800 (TA Instruments) equipped with compression clamp (40 mm discs diameter) in isothermal conditions (25°C) and controlled force mode. Specifically, a round shape sample (diameter *ca.* 30 mm and thickness *ca.* 5 mm) was compressed applying a preload of 0.005 N and with a force ramp rate of 1 $N \cdot min^{-1}$. The compressive modulus was determined from the slope of the linear elastic region, between a strain of 0.5 and 1.0 %, of the stress–strain curves.

X-ray diffraction (XRD) measurements were performed by a PANalytical Empyrean X-ray diffractometer equipped with a 1.8kW CuKα ceramic X-ray tube (λ = 1.5418 Å), PIXcel^{3D}area detector (2×2 mm^2) and operating at 45 kV and 40 mA. The characterizations were performed in air and at room temperature, in parallel-beam geometry and symmetric reflection mode (range 25° – 70° 2θ, step time of 450 sec, and step size of 0.1°), repeating the measurement four times in order to reduce the signal noise. All results were further processed by using PANalytical HighScore 4.1 software. The average crystallites size was estimated by applying the Scherrer equation on the XRD data. The detailed procedure is reported in the supporting information file.

Molecular weights were determined by gel permeation chromatography (GPC) with an Agilent 1260 Infinity instrument (G1322A 1260 Degasser, G1310B 1260 Isocratic Pump, G1316A 1260 TCC Thermostatted Column Compartment, G1362A 126 RID Reflective Index Detector, G1328C 126 Manual Injector); RID and column compartment were thermostatically controlled at 35°C ± 0.2°C. The instrument was equipped with a PLgel MiniMIX-A column (20 µm particle size, 4.6×250 mm) coupled with a Tosoh TSKgel SuperMultipore HZ-M column (4 µm particle size, 4.6×150 mm); columns were preceded by a low dispersion in-line filter (frit porosity 0.2 µm). $CHCl_3$ was used as mobile phase at a flow rate of 0.2 $mL \cdot min^{-1}$ and toluene was used as internal standard (0.1 $\mu L \cdot mL^{-1}$), run time of 37 minutes. Data were processed with Agilent GPC/SEC software, version A.02.01 using a calibration curve obtained with monodispersed polystyrene standards (EasiCal PS-1 Agilent kit).

Thermal properties of the prepared materials were evaluated by differential scanning calorimetry (DSC, Q10, TA Instruments), fitted with a standard DSC cell, and equipped with a Discovery Refrigerated Cooling System (RCS90, TA Instruments). Measurements were performed under dry nitrogen flow (50 $mL \cdot min^{-1}$) on samples of approximately 6 mg, placed in an aluminum pan. The samples were analyzed applying thermal cycle from -40°C to 195°C (hold for 1 min) with a heating rate of 20°C·min^{-1} and a cooling rate of 10°C·min^{-1}. DCS curves

were analyzed by TA Universal Analysis 2000 in order to extrapolate crystallization temperature and melting temperature from the main peak of the first heating and cooling scans.

The actual contents of HA in the composite scaffolds were determined by thermogravimetric analysis (TGA, Q50, TA Instruments), as residual weight after polymer decomposition. Analyses were performed under dry nitrogen flow (60 mL·min^{-1}) on samples of about 20 mg, placed in platinum pans. The sample was heated from room temperature to 700°C with a rate of 10°C·min^{-1}. Degradation temperatures (T_{deg}) were determined as the temperature corresponding to the maximum of the derivative weight loss curves.

The open porosity (P_0) of the scaffolds was evaluated adjusting the standard methodology UNI EN 1936:2007,[33] as previously reported.[30] Briefly, a whole scaffold was dried overnight at 70°C in an oven and consecutively weighted to obtain the dry mass (m_d). Next, the sample was placed in a high-vacuum vessel and the pressure was slowly decreased up to 20 mbar and kept for 5 h. Milli Q water was then gradually introduced into the vessel, maintaining the pressure at 20 mbar. After 1 h, when the scaffold was completely immersed in water, the pressure was returned to the atmospheric one and maintained for 24 h. The sample was then weighted in water (hydrostatic mass, m_h). Finally, the scaffold was gently blotted with a dampened tissue paper and weighted to obtain the saturated mass (m_s). The P_0 was calculated by the following equation:

$$P_0 = (m_s - m_d)/(m_s - m_h) \times 100 \qquad \text{Equation 1}$$

The measurement was carried out on tree samples for each analyzed scaffold.

In order to investigate the ability to support cell growth and differentiation for bone tissue regeneration, preliminary *in vitro* biological investigations were carried out on PHB/HA composites. Among all the prepared compositions, *ex situ* and *in situ* composites with a filler content of 2% and 5% were chosen together with neat PHB for comparison. Mouse calvaria pre-osteoblast MC3T3-E1 cell line (CRL-2594) was selected. Cells were purchased from American Type Culture Collection (ATCC) and propagated using Minimum Essential Medium *alpha* modification (α-MEM), supplemented with 2 mM of L-glutamine, 1% of penicillin: streptomycin solution (10,000 U·mL^{-1} : 10 mg·mL^{-1}), 10% of fetal bovine serum and antimycotic (complete α-MEM). PHB/HA samples were cut into pieces of about 0.5 cm^3 and sterilized by exposure to UV light for 30 minutes and consecutively covered with ethanol/water solution (70%) for 24 hours. Afterwards, samples were extensively washed with Dulbecco's Phosphate Buffer Saline (DPBS) added with penicillin/streptomycin solution (1%) in order to remove ethanol residues and pre-incubated for additional 24 hours with complete α-MEM. The sterilized

samples were then placed into a 24 wells culture plate, seeded with MC3T3-E1 cells (passage 29) at a concentration of $1x10^5$ and incubated 37°C in a 5% CO_2 enriched atmosphere. MC3T3-E1 cells cultured on tissue culture polystyrene (TCPS) were used as control. Cells were allowed to proliferate for 24 hours prior to the incubation with osteogenic medium, obtained by adding to the complete α-MEM ascorbic acid γ-irradiated (50 $\mu g \cdot mL^{-1}$) and β-glycerolphosphate disodium salt hydrate (10 mM). Biological investigations were performed at days 7, 14 and 21 after seeding and data are represented as average value ± standard deviation.

Cell proliferation was investigated by mean of Alamar Blue assay. Briefly, cells were incubated with the diluted reagent (1:10) for 24 hours, at 37°C and 5% CO_2. Measurements of resorufin dye absorbance were carried out with a microplate reader at 540 nm, using 595 nm as reference wavelength.

Early osteogenesis markers of cell differentiation were investigated by evaluating alkaline phosphatase (ALP) activity and collagen production by MC3T3-E1 cultured on the scaffolds. ALP was assessed with a colorimetric method based on the enzymatic conversion of *p*-nitrophenyl phosphate into *p*-nitrophenol. Scaffolds were washed three times with DPBS and then placed into 1 mL of *lysis buffer* (pH 10), containing Triton X-100 (0.2%), magnesium chloride (5 mM), trizma base (10 mM), and protease inhibitors cocktail (2.5 $\mu L \cdot mL^{-1}$). Samples were incubated at 4°C for 15 minutes and purified at 13000 rpm for 10 minutes. Afterwards, a solution containing glycine (0.1 M), magnesium chloride (1 mM), zinc chloride (1 mM), and *p*-nitrophenyl phosphate (1 $mg \cdot mL^{-1}$) was added to 100 µL of samples and to pre-fixed concentrations of *p*-nitrophenol. The reaction was allowed to take place at 37°C for 30 minutes and the stopped by adding 50 µL of 2M NaOH solution; the absorbance was measured at 405 nm. The molar concentration of ALP was normalized with the total protein content of each sample, which was measured using BCA protein assay (Pierce). The ALP activity is reported as nanomoles (nmol) of product *per* (mg of protein$\cdot min^{-1}$).

Assessment of collagen production was performed by the dye Direct red 80. Samples were washed twice with DPBS and incubated with a solution of the dye dissolved in picric acid (0.1%), for 1 hour at room temperature. Samples were then washed three times with HCl 10 mM to remove dye excess. The elution of the bound stain was performed with NaOH 0.1 M for 30 minutes at 37°C. Supernatants were plated in 96 wells plate and the absorbance was read at 540 nm. Unseeded scaffolds were treated following the same protocol and considered as blank. The photometric quantification of the collagen was obtained by means of a calibration curve prepared with collagen type I, derived from calf's skin, filmed on glass slides.

Morphology of MC3T3-E1 cells cultured on composite scaffolds was investigated by means of confocal laser scanning microscopy (CLSM) at day 21 of culture. Cells were fixed with 3.8% paraformaldehyde for 1 hour in Phosphate Buffer Saline (PBS 1X) at room temperature and permeabilized with a PBS 1X/Triton X-100 solution (0.1%) for 5 min. After blocking with 1% wt./vol. bovine serum albumin (BSA) in PBS 1X for 30 min, cells were incubated with Phalloidin-Fluorescein Isothiocyanate labelled in 1% BSA in PBS 1X at room temperature in the dark. After 30 min, cells were incubated with a solution of 4'-6-diamidino-2-phenylindole (DAPI) for 5 minutes. After dyeing incubation, samples were extensively washed with PBS 1X before mounting on a glass slide for microscopic observation. A Nikon Eclipse TE2000 inverted microscope equipped with EZ-C1 confocal laser (Nikon, Japan) and Differential Interference Contrast (DIC) apparatus with 20× and 60× oil-immersion objectives were used to analyze the samples. A 405 nm laser diode and an Argon ion laser (488 nm emission) were used to excite, respectively, DAPI and FITC fluorophores. Images were captured with Nikon EZ-C1 software with identical settings for each sample. Images were further processed with GIMP (GNU Free Software Foundation) Image Manipulation Software and merged with Nikon ACT-2U Software.

3. Results and Discussion

The porous structure of a scaffold has a key role in order to have an efficient cell proliferation.[34-37] For this reason the porosity of the prepared samples was evaluated by SEM investigations. As shown in Figure 1, from a morphological point of view, the composites present a well-defined porous structure with average pore dimension that decreases when the filler content is increased. In particular, the average pore dimension is approximately of 38±20, 23±8, 37±5 and 12±6 μm for IS_9802, IS_9505, IS_9208 and IS_9010 respectively. In the case of the composite scaffolds ES_9802 and ES_9505 comparable values with the analogous samples prepared by *in situ* method were found, with pore size of 42±10 and 31±12 μm, respectively. On the other hand, it is observed a complete loss of porosity for higher filler content (ES_9208 and ES_9010), which is particularly clear by SEM images in Figure 1, making this approach more limiting compared to the *in situ* one where an appreciable porous structure is maintained up to HA content of 8%.

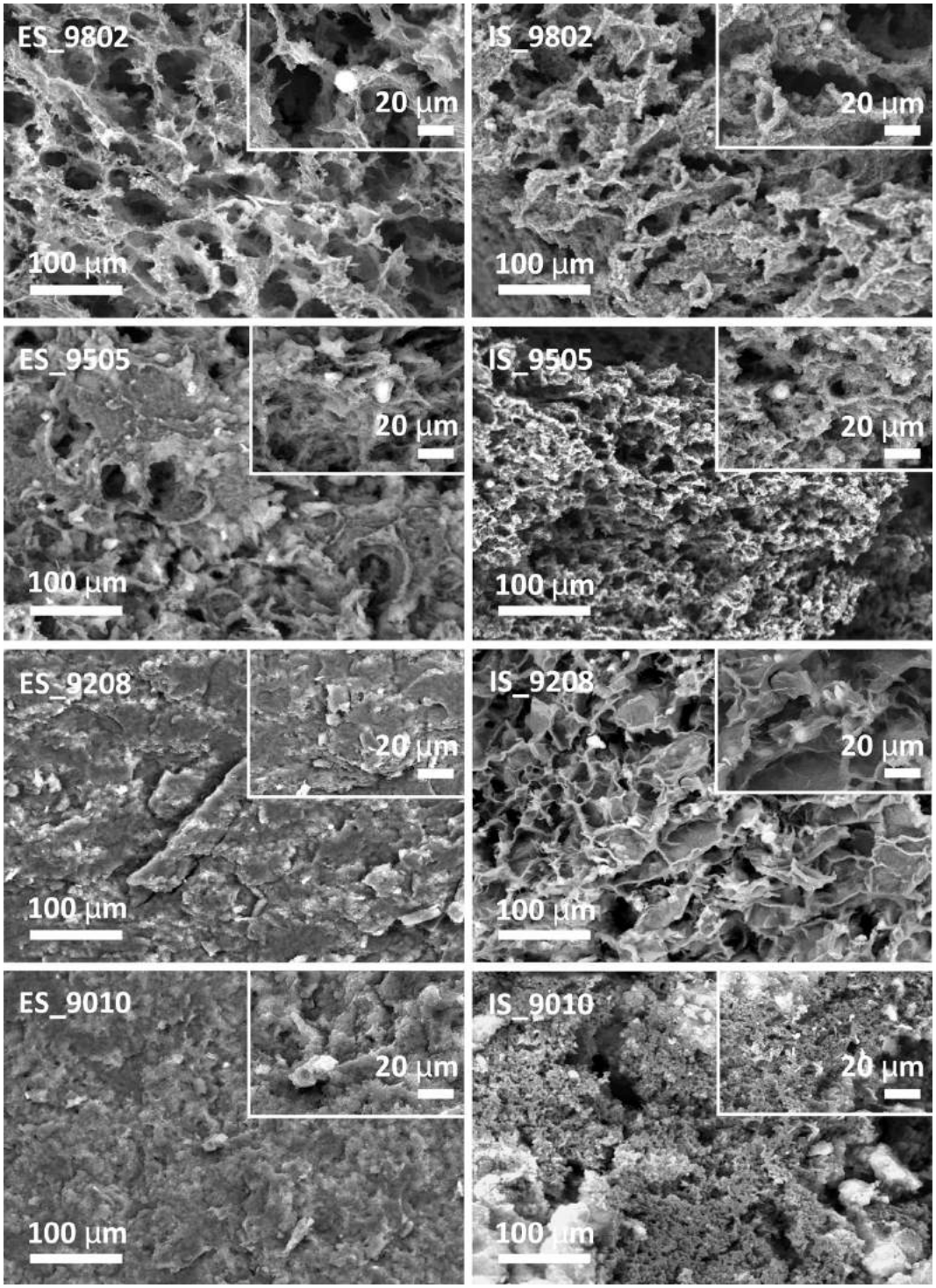

Figure 1. Cross-section SEM micrographs for all prepared PHB/HA composite scaffolds. Higher magnification images are reported in the insets.

The mechanical properties evaluated by compression tests are in good agreement with porous structure observed by SEM investigation (Figure 1). In particular, it was noticed that for all samples with an appreciable porous structure the compressive modulus is not importantly affected by the filler content, showing

comparable values in the range between 2.5 and 5 KPa. On the other hand, when the porosity becomes less evident, as in the case of samples loaded with 10 %wt. of filler (see SEM images in Figure 1), the compressive modulus increases significantly to values of 1889 and 3606 KPa for IS9010 and ES9010, respectively (detailed values reported in table S1). These results strongly suggest that the mechanical properties are only slightly influenced by the material composition, but mainly affected by the degree of porous structure developed during the preparation.

The XRD diffractograms of the bare inorganic particles, reported at the bottom of Figure 2a and 2b, perfectly match with HA hexagonal crystalline structure (Reference code: 96-900-3550) with a Ca/P stoichiometric ratio of 1.66, which is the desired stoichiometry composition of HA in natural bone tissues.[32] Moreover, applying the Scherrer equation to the particle diffractograms, the average crystallites size was calculated (details in supporting information), showing a crystallites dimension that rages from 35 to 46 nm. As shown by the XRD measurements performed on the composites with HA *ex situ* synthesized (Figure 2a) the intensities of the main peaks at 31.7, 32.2 and 32.8°2θ, associated to the reflection of (121), (112) and (030) HA lattice planes (Reference code: 96-900-3550), become more and more intense by increasing the filler content. The same trend is also observed for composites with HA *in situ* synthesized (Figure 2b), in which the main reflections of the inorganic particles arise from the typical PHB diffractogram.[38] Such result indicates that *in situ* process is an effective alternative for introducing an inorganic filler in a polymeric matrix. On the other hand, it strongly suggests that the HA particles formation is not suppressed by the presence of the PHB in the reactive solution, making this method a simple and valuable synthetic procedure to prepare PHB/HA composites.

The morphology of the bare HA particles can be observed in Figure 2c, 2d and 2e, which report the results of the TEM investigations. In particular, HA particles are presented on the grid as small aggregates (Figure 2c), which formation is ascribed to the TEM grid preparation. Although HA particles are organized in small aggregates, it is possible to notice that the primary particles present a rod-like morphology (Figure 2d and 2e) with diameter of 15±7 nm and length of 153±58 nm (both size distributions in Figure S2). Moreover, the EDS analyses (in Figure S3) performed on the particles shown in Figure 2c, 2d and 2e, further support the Ca/P stoichiometric composition observed by XRD measurements.

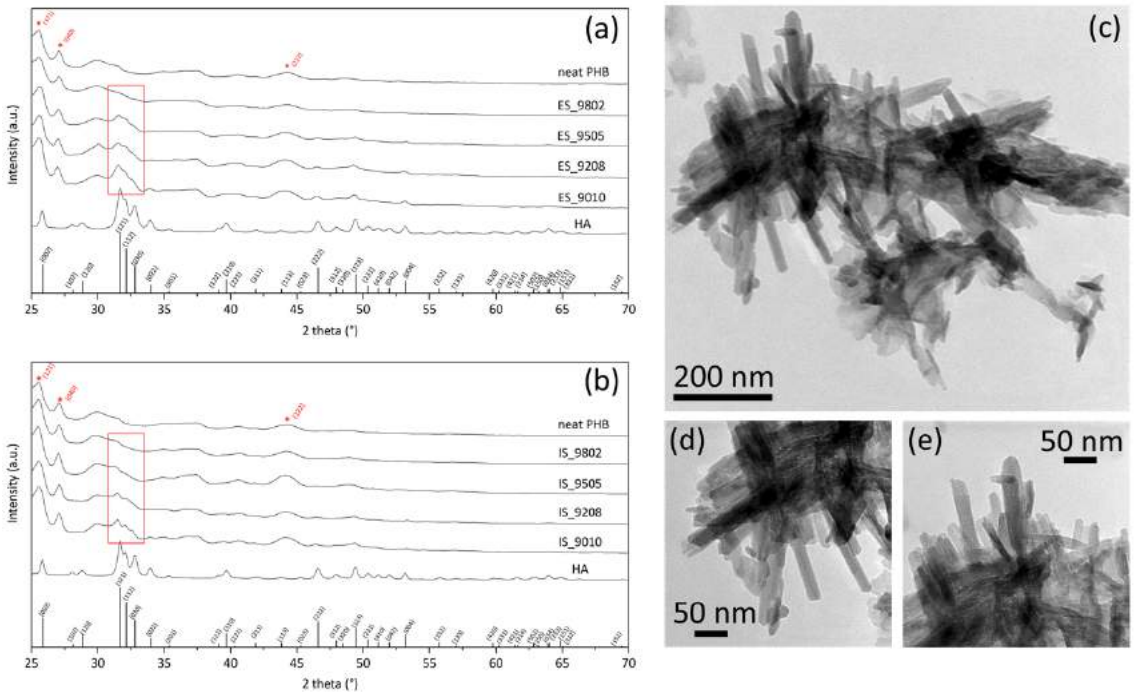

Figure 2. XRD diffractograms of the samples prepared by (a) *ex situ* and (b) *in situ* synthesis method. The solid lines at the bottom describe the patterns of hexagonal hydroxyapatite (ICDD:96-900-3550). Red rectangles highlight the contributions of HA in the composites. Red asterisks (*) describe the contributions due to crystalline portion of PHB.[38] (c, d and e) TEM micrographs of HA at different magnifications.

The actual filler content of each composite was determined by TGA measurements. Figures 3a and 3b show that the determined amounts of filler, for all samples, are very close to the expected ones, indicating that the HA *in situ* formation is characterized by a high reaction yield and an effective method for preparing composite materials. Furthermore, for both sets of samples, T_{deg} extrapolated by derivative weight loss curves (in Figure S4) follows a very similar trend. T_{deg} initially increases up to 5 wt.% of HA and decreases when the filler content is further incremented (Figure 3c). Typically, an increase of T_{deg} is observed when a strong filler/polymer adhesion and/or an improved particle dispersion is observed.[39] This effect is further enhanced by decreasing the average particles size of the filler, which leads to an increased filler/polymer interfacial area. It was reported that when the filler content is increased above 5 wt.%, particles aggregation can occur, which decrease filler/polymer interfacial area and thus the effect on the thermal properties of the composite material.[39, 40] Figure 3c clearly shows that the *in situ* synthesized filler increases more significantly the T_{deg} if compared to the samples prepared by *ex situ* synthesized HA. Such result suggests that the *in situ* approach

leads to a more efficient effect probably due to both filler/polymer adhesion and enhanced filler dispersion thanks to a prevented HA aggregation.[20, 41]

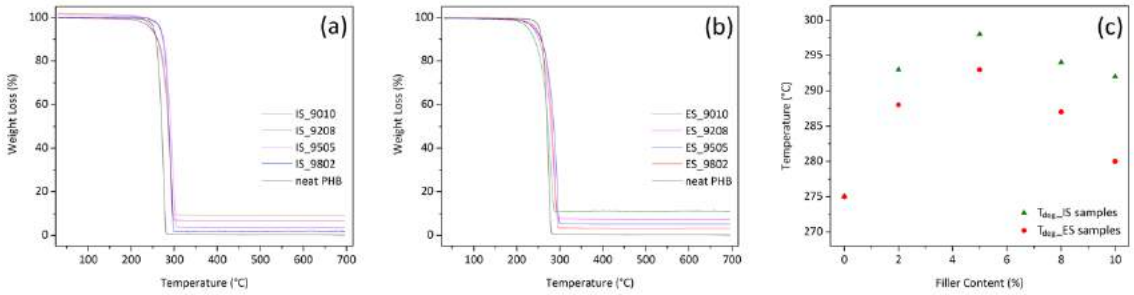

Figure 3. TGA curves of samples prepared by HA (a) *in situ* and (b) *ex situ* synthesized. (c) Degradation temperature (T_{deg}) as a function of the filler content of samples prepared by *in situ* (red dot) and *ex situ* process (green triangle).

This is also confirmed by HRSEM images in Figure 4, which shows that *ex situ* samples present several aggregates despite they are homogeneous distributed. On the other hand, the *in situ* samples showed a remarkably higher dispersion with no sign of HA particles aggregation.

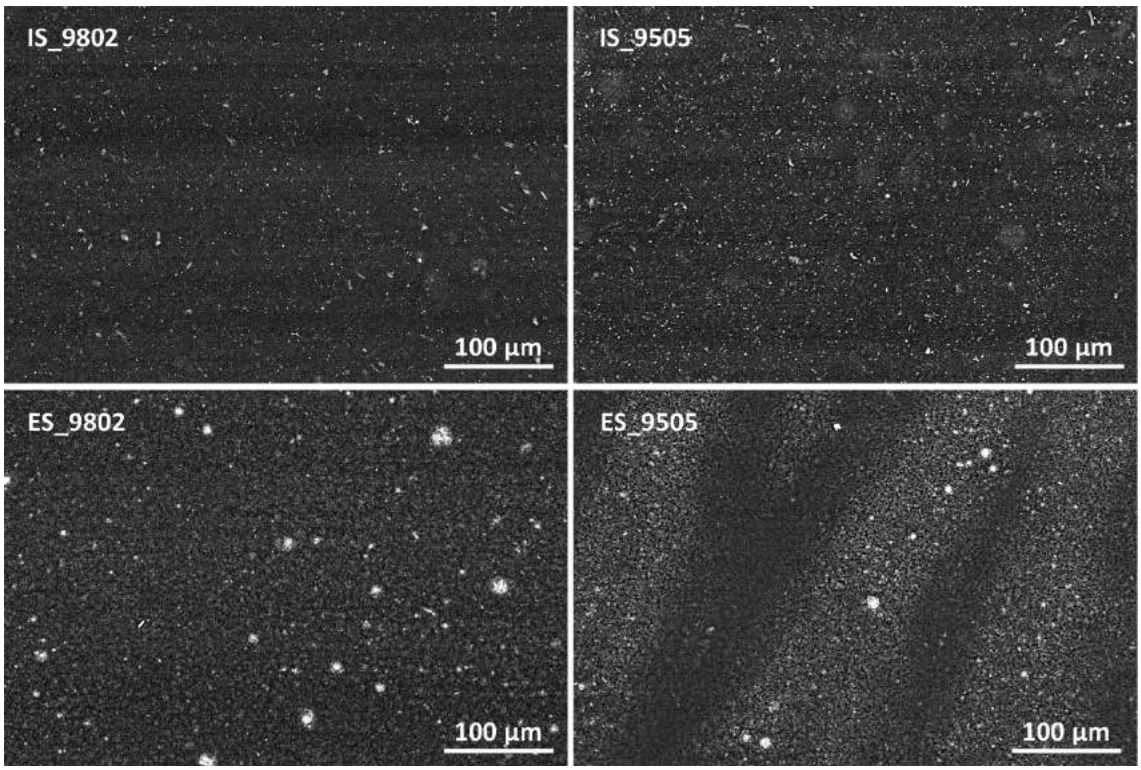

Figure 4. Representative HRSEM images (back-scattered electrons) to highlight the HA particle distribution in the samples IS_9802, IS_9505, ES_9802 and ES_9505.

Molecular weights, determined by GPC (chromatograms in Figures S5), are summarized in Table 2. Specifically, a bimodal distribution is observed for all samples: at lower elution times, the main fraction of PHB (peak A) is detected and a smaller fraction of lower molecular weights PHB (peak B) is observed at higher elution times (Figure S5). In detail, the purification procedure used for eliminating all the process residual impurities does not significantly affect peak molecular weight (M_p), number average molecular weight (M_n) and weight average molecular weight (M_w) of PHB (more details in Table S2 and Figure S6 of the supporting information). The only variable changed between experimental grade and purified PHB is the A/B ratio (%/%), showing that the purification process removes the very low molecular weights.

By comparing purified PHB with the neat PHB scaffold, it can be observed that the molecular weights and the A/B ratio are similar, indicating that in absence of filler the effect of the sonication on the polymer chains is negligible. On the contrary, in presence of filler, A/B ratio changes due to an increase of B fraction for both *ex situ* compositions and *in situ* synthesized. This rise might be ascribed to the mechanical effect of the solid particles on the polymer chains of peak A and their subsequent break, which leads to an increase in fraction B. M_p, M_n and M_w of both fraction A and B are very similar for all *ex situ* and *in situ* PHBs composites (Table 2). This evidence proves that the *in situ* reaction does not affect the molecular weight of the polymeric matrix for all the prepared compositions (more details in Table S2 and Figure S6).

Furthermore, comparing the molecular weights of purified PHB and *ex situ* and *in situ* samples, it can be observed that in some cases the molecular weights of the PHB-based composites are higher than those of purified PHB used. This in apparently not clear behaviour might be explained by considering the not synthetic origin of the PHB used and that some low variation in terms of molecular weights distribution might be observed and commonly accepted.

Table 2. Molecular weights (M_p, M_n and M_w) as determined by gel permeation chromatography for peak A and B. A/B ratio (%/%) calculated from the maximum intensity of each signal.

		Peak A			Peak B		
Sample	**A/B ratio (%/%)**	**M_p**	**M_n**	**M_w**	**M_p**	**M_n**	**M_w**
Experimental grade PHB	59:41	99800	42400	134700	800	700	800
Purified PHB	96:04	96800	36300	134200	400	600	600
PHB	91:09	80900	38100	106700	700	700	800
ES_9802	54:46	118000	44600	141300	700	700	700
ES_9505	64:36	102000	50200	147600	700	700	800
ES_9208	63:37	108700	42300	138600	700	700	700
ES_9010	61:39	108500	55000	144300	600	600	700
IS_9802	61:39	102900	51700	133100	700	800	800
IS_9505	52:48	107900	48100	127800	700	700	700
IS_9208	56:44	84600	37500	107000	600	600	600
IS_9010	67:33	78200	35000	97000	700	700	800

The low variation of the PHB M_p, M_w and M_n was also confirmed by the DSC results (DSC curves in Figure S7 of supporting information) performed on the prepared samples. Specifically, both T_c and T_{m1} are not significantly affected by the filler content in both type of samples, as shown by Figure 5a and 5b, suggesting that the molecular weight of the polymer is not affected by the HA *in situ* formation process.

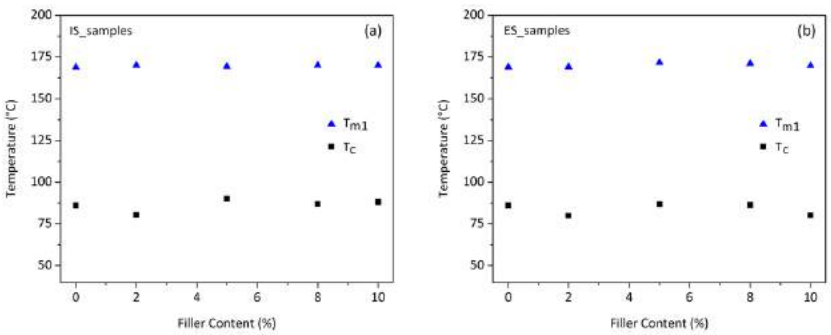

Figure 5. Crystallization temperature (T_c) and melting temperature (T_{m1}) as a function of the filler content of samples prepared by (a) *in situ* and (b) *ex situ* process.

As mentioned above, open and fully interconnected porous architecture with a tailored pore size is a key factor for designing scaffolds. In fact, a suitable porosity is required to permit and promote tissue ingrowth, transportation of nutrients into the scaffold and removal of metabolic wastes resulting from cellular activity.[34-37] Therefore, it is very important to have samples characterized by comparable porosity in order to have reliable evaluations of cell viability and differentiation. Since samples prepared by *ex situ* process showed a significantly suppressed porosity when the filler content is higher than 5 wt.% (see SEM images in Figure 1), scaffolds prepared by both methods and loaded with 2 and 5 wt.% of HA were chosen for biological tests. This is further supported by the measurements of porosity, which show for all the samples used for biological tests a comparable value of open porosity. Specifically, ES_9802 and ES_9505 showed an open porosity of 92%, whereas the samples IS_9802 and IS_9505 showed a slightly higher value of approximately 95% (values in table S3).

The results of MC3T3-E1 cell proliferation monitored at days 7, 14 and 21 after seeding are reported in Figure 6a as cell proliferation (%) normalized to the control (TCPS equal to 100%). As expected, all the investigated samples were able to support MC3T3-E1 cell adhesion and proliferation, confirming the biocompatibility of the prepared composite scaffolds. Specifically, after 21 days, values higher than 50% were achieved with respect to TCPS, except for the sample IS_9505 that revealed a cell proliferation rate of approximately 25%. The cell differentiation ability was evaluated through early markers assessments monitored at 7, 14 and 21 days after seeding. As shown in Figure 6b, all the scaffolds supported the ALP production, suggesting that the differentiation process started between 7 and 14 days of culture. In particular, IS_9505 and ES_9802 showed the highest ALP production with values recorded at day 7 of culture that are two folds higher than TCPS. On the other hand, IS_9802 and neat PHB displayed ALP values comparable to the control, while the ES_9505 sample showed even lower ALP value. Results on collagen production due to pre-osteoblast cells are reported in Figure 6c, which showed that MC3T3-E1 cells cultured on all samples produced increasing amount of collagen during the culturing period. It is worth noting that at day 21 the amount of collagen detected for both *ex situ* composites and neat PHB samples was comprised between 109 and 154 µg, significantly higher than those obtained from cells grown on TCPS (88 µg). On the contrary, collagen obtained from cells grown on *in situ* composite samples reached values similar to the control.

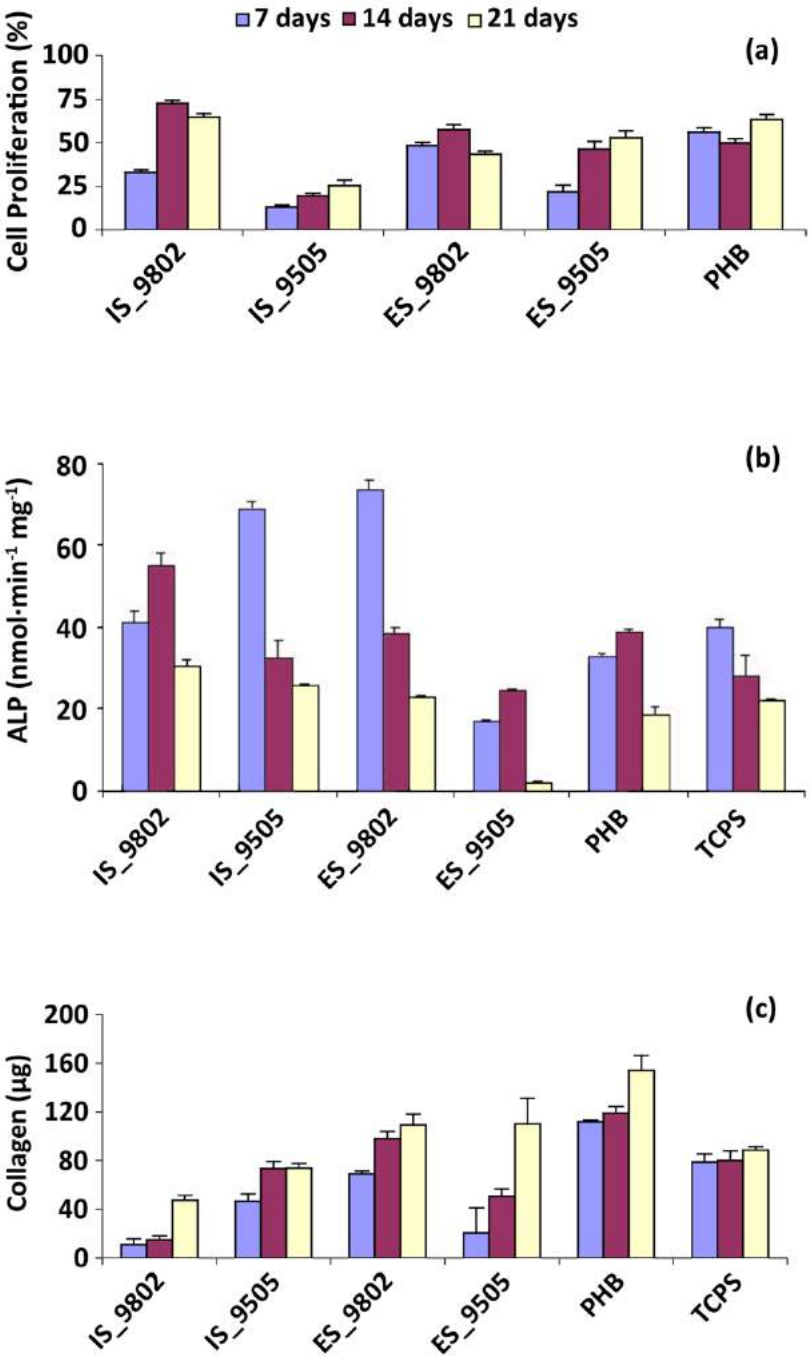

Figure 6. (a) Cell proliferation, (b) ALP activity and (c) collagen production assays from MC3T3-E1 cells cultured on neat PHB and PHB/HA composites scaffolds. TCPS was used as control sample.

Investigations of cell morphology and cytoskeleton organization of MC3T3-E1 cultured on PHB/HA samples were carried out by CLSM analysis. Cells were stained for F-actin and nuclei with FITC-phalloidin and DAPI respectively. After 21 days of culture, microscopic observations showed diffused presence of adherent MC3T3-E1 cells on the surface of neat PHB scaffold (Figures 6a) and PHB/HA scaffolds (Figures 6b, 6c, 6d and 6e). Cell

architecture showed consistent F-actin organization with great stress fibers stretched along the cytoplasm and numerous dendritic extensions from the cell membrane towards the sample's surface (Figures 6b, 6c, 6d and 6e). Moreover, the morphology of cells grown onto neat PHB scaffolds appeared more similar to undifferentiated fibroblasts (Figure 7f). Interestingly, higher magnifications micrographs highlighted the presence of cuboidal cells (Figures 7g, 7h, 7i and 7j), which typically indicates that a of differentiation toward osteoblasts is taking place.

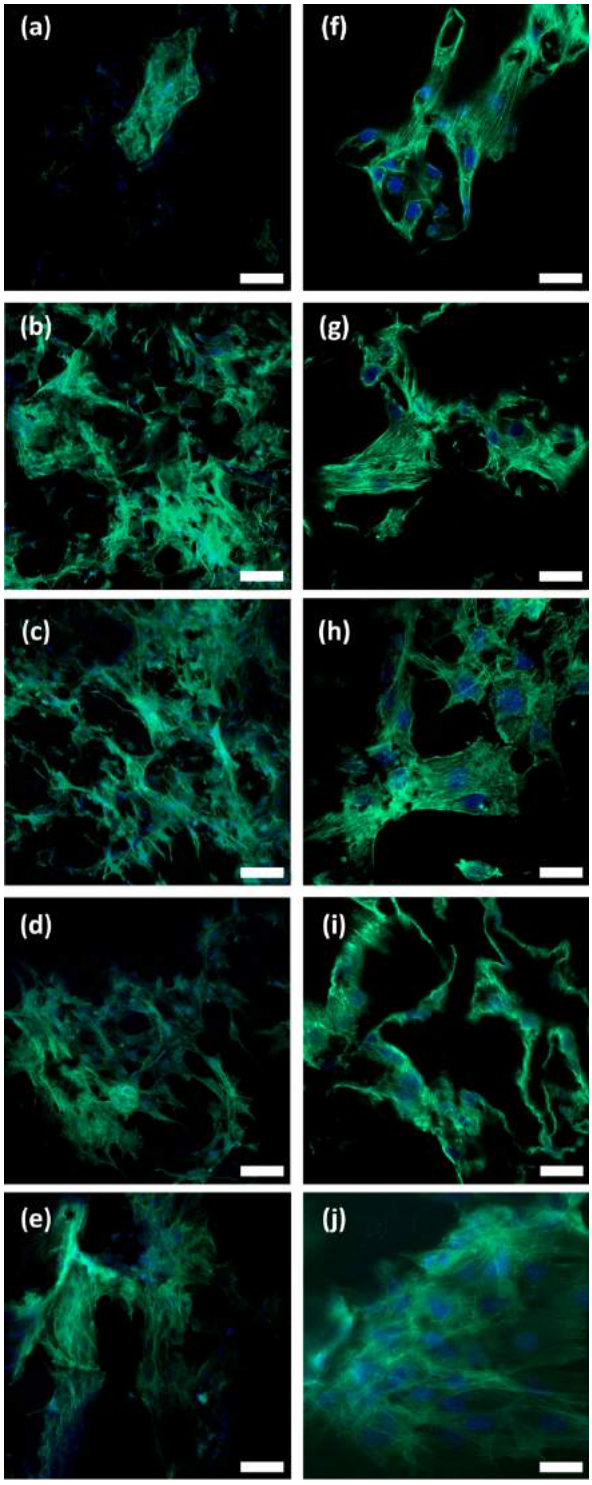

Figure 7. CLSM micrographs of MC3T3-E1 cells grown onto (a) neat PHB, (b) ES_9802, (c) ES_9505, (d) IS_9802, (e) IS_9505 scaffolds (scale bar corresponds to 100 μm). Higher magnification CLSM micrographs of (f) neat PHB, (g) ES_9802, (h) ES_9505, (i) IS_9802, (j) IS_9505 scaffolds (scale bar corresponds to 30 μm).

Considering all the biological assessments, the prepared PHB/HA composites showed different values of cell proliferation depending on HA concentration and the used synthetic approach. In particular, the overall

proliferation measured on 9505 samples resulted lower with respect to the 9802 samples regardless the used synthetic approach (Figure 6a). As reported elsewhere [42], the presence of HA influences the cell differentiation process that is often correlated to a decrease in cell proliferation. This hypothesis is supported by the investigated osteogenesis markers. In fact, the sample IS_9505 showed the highest ALP activity and collagen production (Figures 5b and 5c). Morphological investigations on *in situ* samples further confirmed the quantitative data, showing the presence of cells with morphologies resembling those of both osteoblasts (round or cuboidal shape) and osteocytes (stellate morphology), that are considered to be the terminal differentiation stage of osteoblasts [43] (Figures 6d, 6i, 6e and 6j). Both ES_9802 and ES_9505 exhibit similar values of cell proliferation (Figure 6a). Quantitative data of early markers of osteogenesis highlighted a pronounced ALP activity and collagen production for the ES_9802. On the other hand, for ES_9505 a lower ALP expression and a moderate collagen synthesis were observed (Figures 5b and 5c). Nevertheless, quantitative results of osteogenesis markers obtained for the ES_9505 could be underestimate because of their partial degradation as consequence of the treatment required for the analysis. In fact, investigations on cell morphology revealed that both *ex situ* samples showed differentiated MC3T3-E1 cells with a predominance of osteocytes morphology (Figures 6b, 6g, 6c and 6h). Regarding the neat PHB, a high MC3T3-E1 cell proliferation was observed after 7 day of culture and during the entire culturing period (Figure 6a). Moreover, on neat PHB, MC3T3-E1 produced the highest amount of collagen (Figure 6c). Nevertheless, the low production of ALP (Figure 6b) suggests a weak process of cell differentiation, as also confirmed by CLSM micrographs. In fact, confocal analysis (Figure 7a and 7f) revealed the presence of a heterogeneous population formed mainly by spindle-shaped MC3T3-E1, resembling undifferentiated preosteoblast cells.

4. Conclusions

Composite porous scaffolds based on poly(3-hydroxybutyrate), obtained from sugar cane and beet agro-wastes, have been successfully functionalized with hydroxyapatite by means of *in situ* and *ex situ* synthesis in order to promote the osteogenesis. In particular, the innovative *in situ* approach is based on the formation of crystalline hydroxyapatite in presence of the polymeric matrix in the reaction medium. Such approach limits the particle aggregation that typical occurs when an inorganic filler is *ex situ* synthesized and consecutively

redispersed in a polymeric matrix. Interestingly, the evolution of the porous structure by thermally induced phase separation technique, is strongly suppressed by the presence of high content of hydroxyapatite. This occurs especially when the *ex situ* synthesized particles are dispersed by conventional mixing methods, therefore limiting the use of this approach for preparing porous scaffolds. On the other hand using the *in situ* method the porosity formation is preserved up to a filler content of 8 wt.%, thus allowing to obtain both high hydroxyapatite content and porosity. GPC measurements showed that the *in situ* filler formation process does not affect the poly(3-hydroxybutyrate) molecular weight making the proposed *in situ* approach a very efficient a valuable alternative to the conventional mixing methods to prepare polymer based composites.

Preliminary *in vitro* biological investigations carried out on poly(3-hydroxybutyrate)/hydroxyapatite composites indicated a total lack of toxicity and highlighted the suitability of the scaffolds to sustain MC3T3-E1 cell adhesion and proliferation. In addition, as a result of the morphological cell assessment, all the composites were able to promote MC3T3-E1 cell differentiation towards an osteoblastic phenotype. In particular, cell morphology investigations showed that PHB/HA scaffolds promote differentiation towards osteoblastic phenotype, which was not found for neat PHB scaffolds. This aspect is further supported by the evaluation of the early osteogenic markers. In particular, samples loaded with HA *in situ* synthesized showed the highest ALP production and typical morphology of the terminal differentiation stage of osteoblasts. Future developments will be focused on the bioactivity of the scaffolds in order to better understand the osteoinductivity behaviour as a function of the composition and the method used for the composite preparation.

The herein proposed fabrication procedure can be further extended to other polymeric matrices or different inorganic nanoparticles, opening up an innovative, simple and scalable tool for the preparation of high surface area polymer-based composites with tailored properties.

Acknowledgements

The authors acknowledge Mr Emanuele Guzzi for the technical support on the samples preparation, Dr. Mauro Zapparoli for the technical support on SEM investigations and Dr. Cristina Bartoli for the contribution to the biological evaluation. Furthermore, we greatly acknowledge Bio-on SpA (Bologna, Italy) for providing experimental grade PHB powder.

Funding

This research did not receive any specific grant from funding agencies in the public, commercial, or not-for-profit sectors.

Supporting Information

Experimental details and more characterizations of the presented materials are reported in the supporting information file.

The authors declare no competing financial interest.

Graphical Abstract

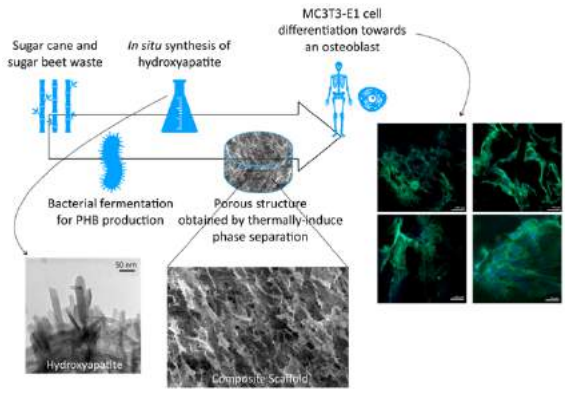

References

[1] L. Roseti, V. Parisi, M. Petretta, C. Cavallo, G. Desando, I. Bartolotti, B. Grigolo, Scaffolds for Bone Tissue Engineering: State of the art and new perspectives, Materials Science & Engineering C-Materials for Biological Applications, 78 (2017) 1246-1262. https://doi.org/10.1016/j.msec.2017.05.017.

[2] B.P. Chan, K.W. Leong, Scaffolding in tissue engineering: general approaches and tissue-specific considerations, European Spine Journal, 17 (2008) 467-479. https://doi.org/10.1007/s00586-008-0745-3.

[3] C.J. Shuai, W. Guo, P. Wu, W.J. Yang, S. Hu, Y. Xia, P. Feng, A graphene oxide-Ag co-dispersing nanosystem: Dual synergistic effects on antibacterial activities and mechanical properties of polymer scaffolds, Chem Eng J, 347 (2018) 322-333. https://doi.org/10.1016/j.cej.2018.04.092.

[4] I. Armentano, M. Dottori, E. Fortunati, S. Mattioli, J.M. Kenny, Biodegradable polymer matrix nanocomposites for tissue engineering: A review, Polym Degrad Stabil, 95 (2010) 2126-2146. https://doi.org/10.1016/j.polymdegradstab.2010.06.007.

[5] C.D. Gao, S.P. Peng, P. Feng, C.J. Shuai, Bone biomaterials and interactions with stem cells, Bone Res, 5 (2017). https://doi.org/10.1038/boneres.2017.59.

[6] P. Wutticharoenmongkol, P. Pavasant, P. Supaphol, Osteoblastic phenotype expression of MC3T3-E1 cultured on electrospun polycaprolactone fiber mats filled with hydroxyapatite nanoparticles, Biomacromolecules, 8 (2007) 2602-2610. https://doi.org/10.1021/bm700451p.

[7] A.P. Marques, R.L. Reis, Hydroxyapatite reinforcement of different starch-based polymers affects osteoblast-like cells adhesion/spreading and proliferation, Materials Science & Engineering C-Biomimetic and Supramolecular Systems, 25 (2005) 215-229. https://doi.org/10.1016/j.msec.2005.01.013.

[8] L. Shor, S. Guceri, X. Wen, M. Gandhi, W. Sun, Fabrication of three-dimensional polycaprolactone/hydroxyapatite tissue scaffolds and osteoblast-scaffold interactions in vitro, Biomaterials, 28 (2007) 5291-5297. https://doi.org/10.1016/j.biomaterials.2007.08.018.

[9] P. Feng, P. Wu, C.D. Gao, Y.W. Yang, W. Guo, W.J. Yang, C.J. Shuai, A Multimaterial Scaffold With Tunable Properties: Toward Bone Tissue Repair, Adv Sci, 5 (2018) 1700817. https://doi.org/10.1002/advs.201700817.

[10] N. Goonoo, A. Bhaw-Luximon, P. Passanha, S.R. Esteves, D. Jhurry, Third generation poly(hydroxyacid) composite scaffolds for tissue engineering, Journal of Biomedical Materials Research Part B-Applied Biomaterials, 105B (2017) 1667-1684. https://doi.org/10.1002/jbm.b.33674.

[11] R.W. Lenz, R.H. Marchessault, Bacterial polyesters: Biosynthesis, biodegradable plastics and biotechnology, Biomacromolecules, 6 (2005) 1-8. https://doi.org/10.1021/bm049700c.

[12] G.Q. Chen, A microbial polyhydroxyalkanoates (PHA) based bio- and materials industry, Chem Soc Rev, 38 (2009) 2434-2446. https://doi.org/10.1039/b812677c.

[13] A.A. Khardenavis, M.S. Kumar, S.N. Mudliar, T. Chakrabarti, Biotechnological conversion of agro-industrial wastewaters into biodegradable plastic, poly beta-hydroxybutyrate, Bioresource Technology, 98 (2007) 3579-3584. https://doi.org/10.1016/j.biortech.2006.11.024.

[14] R. Petkewich, Technology Solutions: Microbes manufacture plastic from food waste, Environ Sci Technol, 37 (2003) 175A-176A. https://doi.org/10.1021/es032456x.

[15] Z. Li, J. Yang, X.J. Loh, Polyhydroxyalkanoates: opening doors for a sustainable future, Npg Asia Materials, 8 (2016). https://doi.org/10.1038/am.2016.48.

[16] G.Q. Chen, Q. Wu, The application of polyhydroxyalkanoates as tissue engineering materials, Biomaterials, 26 (2005) 6565-6578. https://doi.org/10.1016/j.biomaterials.2005.04.036.

[17] C. Ao, Y. Niu, X. Zhang, X. He, W. Zhang, C. Lu, Fabrication and characterization of electrospun cellulose/nano-hydroxyapatite nanofibers for bone tissue engineering, Int J Biol Macromol, 97 (2017) 568-573. https://doi.org/10.1016/j.ijbiomac.2016.12.091.

[18] P. Fabbri, F. Bondioli, M. Messori, C. Bartoli, D. Dinucci, F. Chiellini, Porous scaffolds of polycaprolactone reinforced with in situ generated hydroxyapatite for bone tissue engineering, Journal of Materials Science-Materials in Medicine, 21 (2010) 343-351. https://doi.org/10.1007/s10856-009-3839-5.

[19] M. Oner, B. Ilhan, Fabrication of poly(3-hydroxybutyrate-co-3-hydroxyvalerate) biocomposites with reinforcement by hydroxyapatite using extrusion processing, Materials Science & Engineering C-Materials for Biological Applications, 65 (2016) 19-26. https://doi.org/10.1016/j.msec.2016.04.024.

[20] D. Morselli, F. Bondioli, M. Sangermano, M. Messori, Epoxy networks reinforced with TiO_2 generated by nonhydrolytic sol–gel process: A comparison between in situ and ex situ syntheses to obtain filled polymers, Polymer Engineering & Science, 55 (2014) 1689–1697. https://doi.org/10.1002/pen.24007.

[21] Y.Z. Wan, Y. Huang, C.D. Yuan, S. Raman, Y. Zhu, H.J. Jiang, F. He, C. Gao, Biomimetic synthesis of hydroxyapatite/bacterial cellulose nanocomposites for biomedical applications, Materials Science & Engineering C-Biomimetic and Supramolecular Systems, 27 (2007) 855-864. https://doi.org/10.1016/j.msec.2006.10.002.

[22] Y.Z. Wan, L. Hong, S.R. Jia, Y. Huang, Y. Zhu, Y.L. Wang, H.J. Jiang, Synthesis and characterization of hydroxyapatite-bacterial cellulose nanocomposites, Compos Sci Technol, 66 (2006) 1825-1832. https://doi.org/10.1016/j.compscitech.2005.11.027.

[23] D. Morselli, F. Bondioli, M. Fiorini, M. Messori, Poly(methyl methacrylate)–TiO_2 nanocomposites obtained by non-hydrolytic sol–gel synthesis: the innovative tert-butyl alcohol route, J Mater Sci, 47 (2012) 7003-7012. https://doi.org/10.1007/s10853-012-6651-4.

[24] M. Mehrabanian, D. Morselli, G. Caputo, A. Scarpellini, F. Palazon, A. Athanassiou, D. Fragouli, Laser-induced in situ synthesis of Pd and Pt nanoparticles on polymer films, Applied Physics A, 122 (2016) 1075. https://doi.org/10.1007/s00339-016-0606-6.

[25] M. Mehrabanian, D. Fragouli, D. Morselli, A. Scarpellini, G. Anyfantis, A. Athanassiou, Laser-induced localized formation of silver nanoparticles on chitosan films: study on particles size and density variation, Materials Research Express, 2 (2015) 105014. https://doi.org/10.1088/2053-1591/2/10/105014.

[26] D. Morselli, P. Valentini, G. Perotto, A. Scarpellini, P.P. Pompa, A. Athanassiou, D. Fragouli, Thermally-induced in situ growth of ZnO nanoparticles in polymeric fibrous membranes, Compos Sci Technol, 149 (2017) 11-19. https://doi.org/https://doi.org/10.1016/j.compscitech.2017.05.025.

[27] D. Morselli, A. Scarpellini, A. Athanassiou, D. Fragouli, Single step in situ formation of porous zinc oxide/PMMA nanocomposites by pulsed laser irradiation: kinetic aspects and mechanisms, RSC Advances, 6 (2016) 11412-11418. https://doi.org/10.1039/C5RA23125F.

[28] D. Morselli, F. Bondioli, A.S. Luyt, T.H. Mokhothu, M. Messori, Preparation and characterization of EPDM rubber modified with in situ generated silica, J Appl Polym Sci, 128 (2013) 2525-2532. https://doi.org/10.1002/app.38566.

[29] H.-Q. Liang, Q.-Y. Wu, L.-S. Wan, X.-J. Huang, Z.-K. Xu, Thermally induced phase separation followed by in situ sol-gel process: A novel method for PVDF/SiO2 hybrid membranes, Journal of Membrane Science, 465 (2014) 56-67. https://doi.org/10.1016/j.memsci.2014.03.068.

[30] M.G. Gandolfi, F. Zamparini, M. Degli Esposti, F. Chiellini, C. Aparicio, F. Fava, P. Fabbri, P. Taddei, C. Prati, Polylactic acid-based porous scaffolds doped with calcium silicate and dicalcium phosphate dihydrate designed for biomedical application, Materials Science & Engineering C-Materials for Biological Applications, 82 (2018) 163-181. https://doi.org/10.1016/j.msec.2017.08.040.

[31] D.M. Liu, T. Troczynski, W.J. Tseng, Water-based sol-gel synthesis of hydroxyapatite: process development, Biomaterials, 22 (2001) 1721-1730. https://doi.org/10.1016/S0142-9612(00)00332-X.

[32] I. Bogdanoviciene, A. Beganskiene, K. Tõnsuaadu, J. Glaser, H.J. Meyer, A. Kareiva, Calcium hydroxyapatite, $Ca_{10}(PO_4)6(OH)_2$ ceramics prepared by aqueous sol–gel processing, Mater Res Bull, 41 (2006) 1754-1762. https://doi.org/10.1016/j.materresbull.2006.02.016.

[33] Standard UNI EN 1936:2007, Natural stone test methods - Determination of real density and apparent density, and of total and open porosity, Ente Nazionale Italiano di Unificazione, 2007.

[34] J. Voorneveld, A. Oosthuysen, T. Franz, P. Zilla, D. Bezuidenhout, Dual electrospinning with sacrificial fibers for engineered porosity and enhancement of tissue ingrowth, Journal of Biomedical Materials Research Part B-Applied Biomaterials, 105B (2017) 1559-1572. https://doi.org/10.1002/jbm.b.33695.

[35] C. Vitale-Brovarone, E. Verne, L. Robiglio, P. Appendino, F. Bassi, G. Martinasso, G. Muzio, R. Canuto, Development of glass-ceramic scaffolds for bone tissue engineering: Characterisation, proliferation of human osteoblasts and nodule formation, Acta Biomaterialia, 3 (2007) 199-208. https://doi.org/10.1016/j.actbio.2006.07.012.

[36] K. Rezwan, Q.Z. Chen, J.J. Blaker, A.R. Boccaccini, Biodegradable and bioactive porous polymer/inorganic composite scaffolds for bone tissue engineering, Biomaterials, 27 (2006) 3413-3431. https://doi.org/10.1016/j.biomaterials.2006.01.039.

[37] G.J. Bassi AK, Zakikhani M, Downes S, Bone tissue regeneration, in: D.S. Bosworth L (Ed.) Electrospinning for Tissue Regeneration, Woodhead Publishing, Cambridge, UK, 2011, pp. 93-110.

[38] P. Anbukarasu, D. Sauvageau, A. Elias, Tuning the properties of polyhydroxybutyrate films using acetic acid via solvent casting, Sci Rep-Uk, 5 (2015). https://doi.org/10.1038/srep17884.

[39] J. Seo, G. Jeon, E.S. Jang, S.B. Khan, H. Han, Preparation and Properties of Poly(propylene carbonate) and Nanosized ZnO Composite Films for Packaging Applications, J Appl Polym Sci, 122 (2011) 1101-1108. https://doi.org/Doi 10.1002/App.34248.

[40] K. Paderni, D. Morselli, F. Bondioli, A.S. Luyt, T.H. Mokhothu, M. Messori, EPDM rubber reinforced with titania generated by nonhydrolytic sol-gel process, Polymer Engineering & Science, 54 (2013) 2544-2552. https://doi.org/10.1002/pen.23805.

[41] A. Spinella, F. Bondioli, G. Nasillo, V. Renda, E. Caponetti, M. Messori, D. Morselli, Organic-inorganic nanocomposites prepared by reactive suspension method: investigation on filler/matrix interactions and their

effect on the nanoparticles dispersion, Colloid Polym Sci, 295 (2017) 695-701. https://doi.org/10.1007/s00396-017-4036-6.

[42] R. Shu, R. McMullen, M.J. Baumann, L.R. McCabe, Hydroxyapatite accelerates differentiation and suppresses growth of MC3T3-E1 osteoblasts, Journal of Biomedical Materials Research Part A, 67A (2003) 1196-1204. https://doi.org/10.1002/jbm.a.20021.

[43] H. Nakamura, Morphology, Function, and Differentiation of Bone Cells, Journal of Hard Tissue Biology, 16 (2007) 15-22. https://doi.org/10.2485/jhtb.16.15.

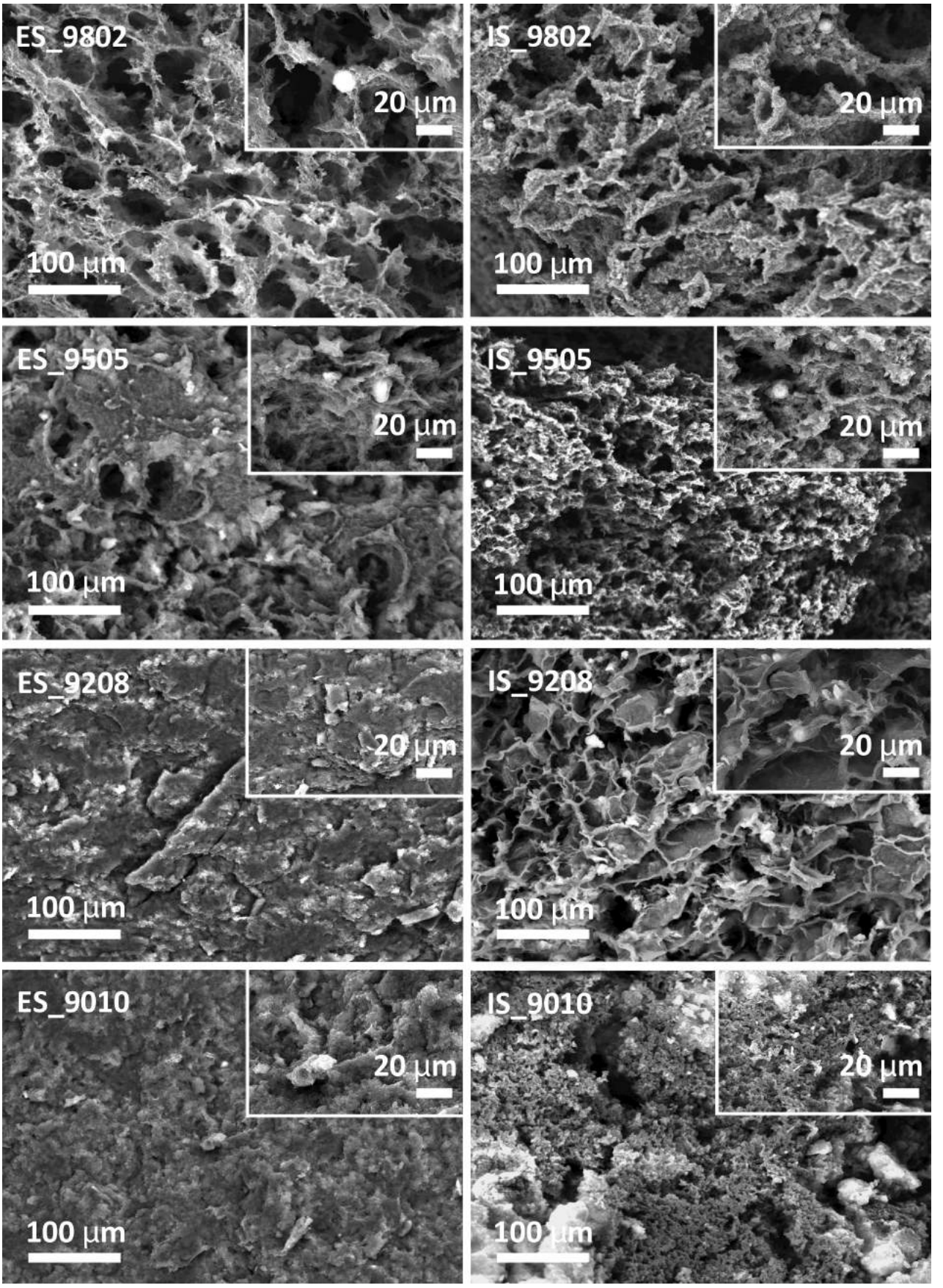
ES_9802
20 μm
100 μm
IS_9802
20 μm
100 μm
ES_9505
20 μm
100 μm
IS_9505
20 μm
100 μm
ES_9208
20 μm
100 μm
IS_9208
20 μm
100 μm
ES_9010
20 μm
100 μm
IS_9010
20 μm
100 μm

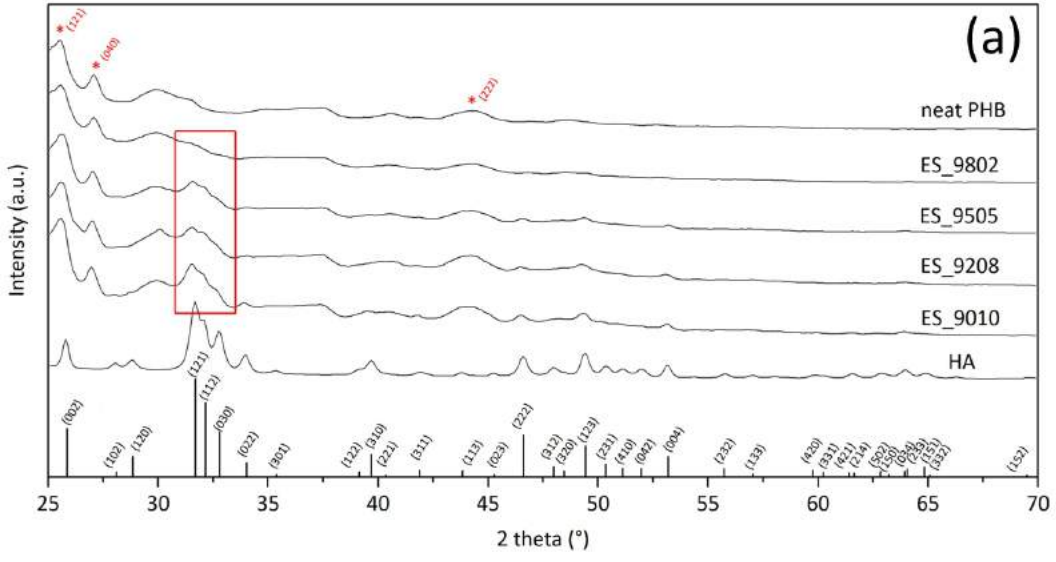
(a)
neat PHB
ES_9802
ES_9505
ES_9208
ES_9010
HA
Intensity (a.u.)
2 theta (°)

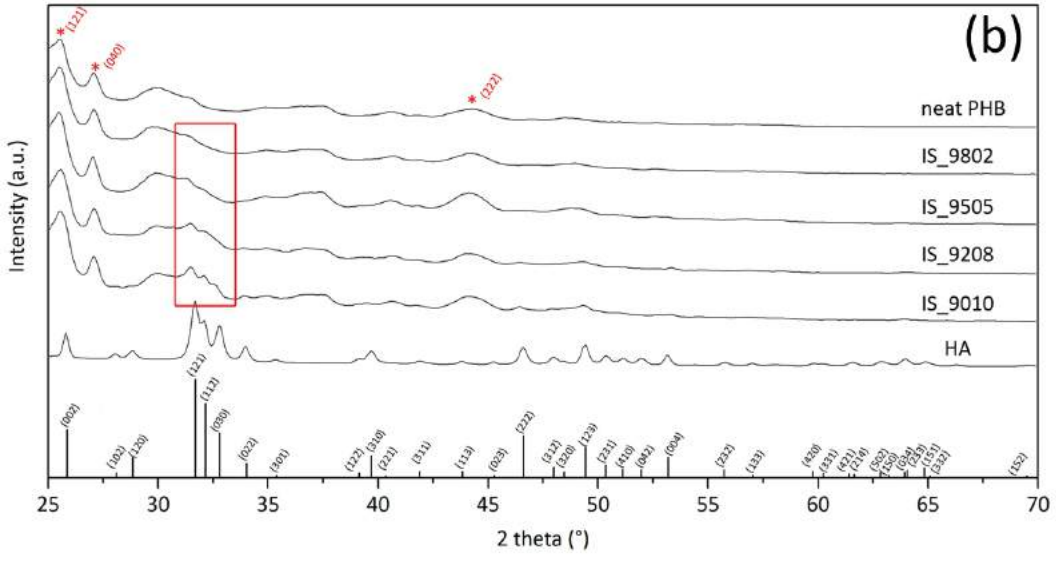
(b)
neat PHB
IS_9802
IS_9505
IS_9208
IS_9010
HA
Intensity (a.u.)
2 theta (°)

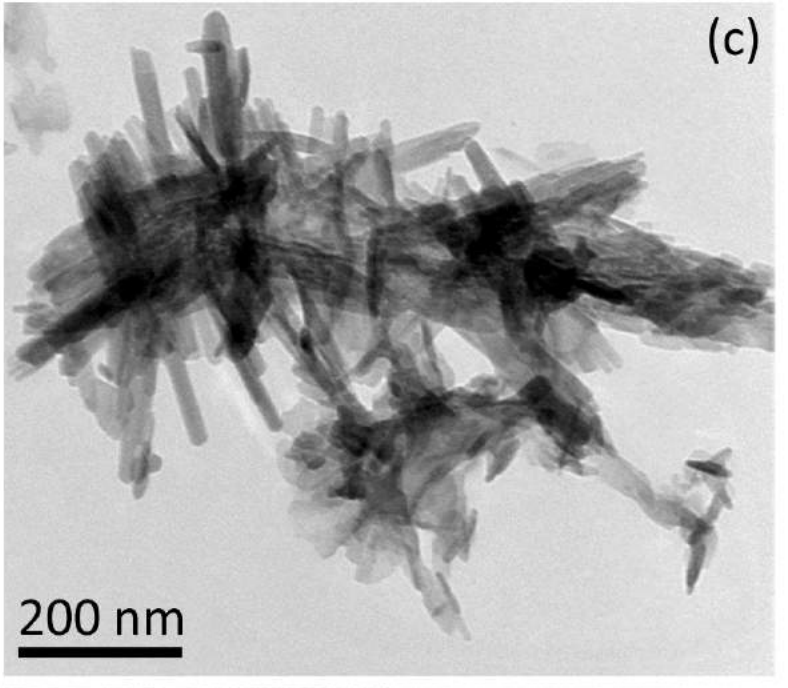
(c)
200 nm

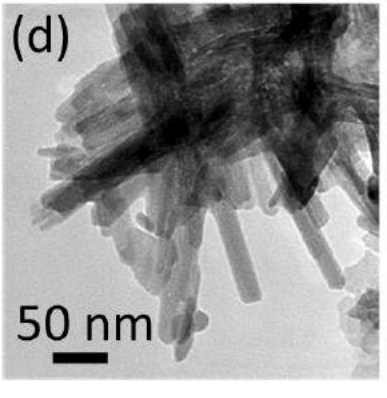
(d)
50 nm

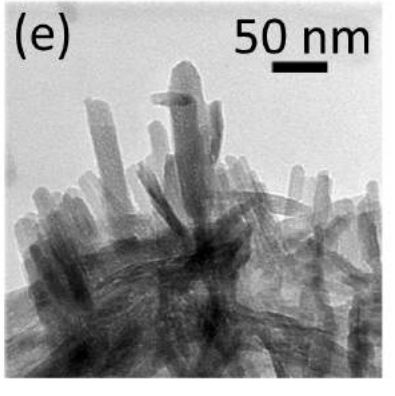
(e)
50 nm

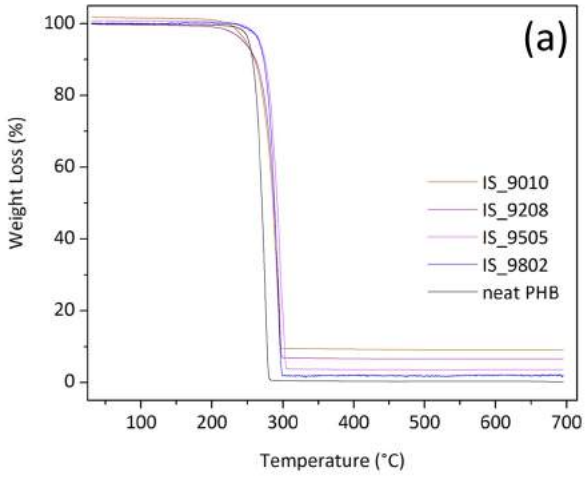
(a)
Weight Loss (%)
Temperature (°C)
IS_9010
IS_9208
IS_9505
IS_9802
neat PHB

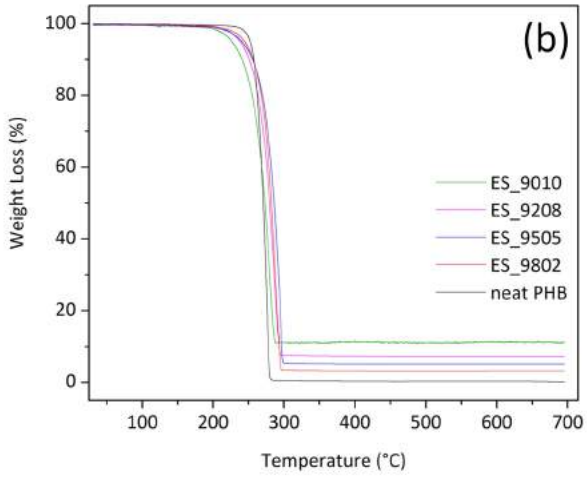
(b)
Weight Loss (%)
Temperature (°C)
ES_9010
ES_9208
ES_9505
ES_9802
neat PHB

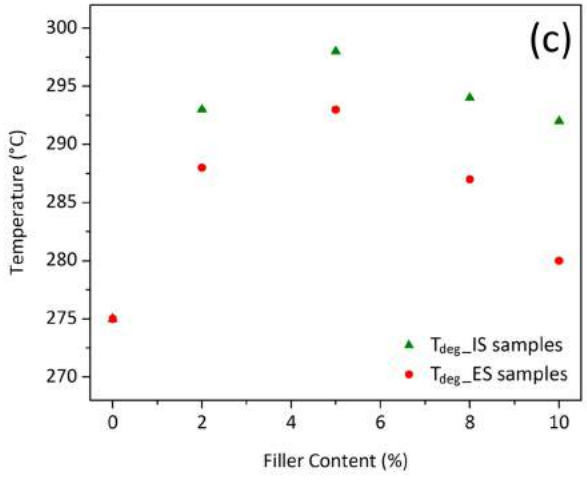
(c)
Temperature (°C)
Filler Content (%)
T_deg_IS samples
T_deg_ES samples

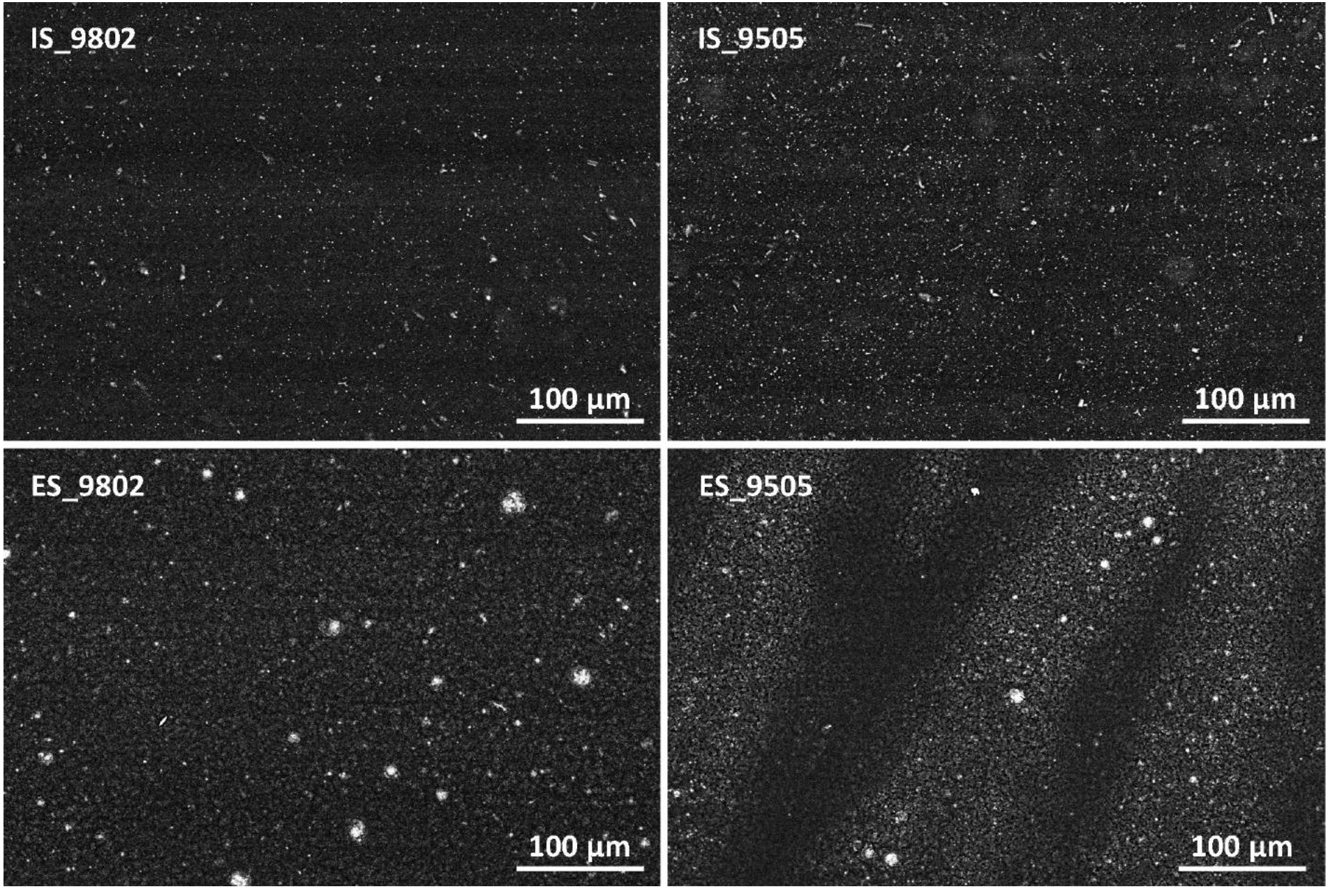
IS_9802
100 µm
IS_9505
100 µm
ES_9802
100 µm
ES_9505
100 µm

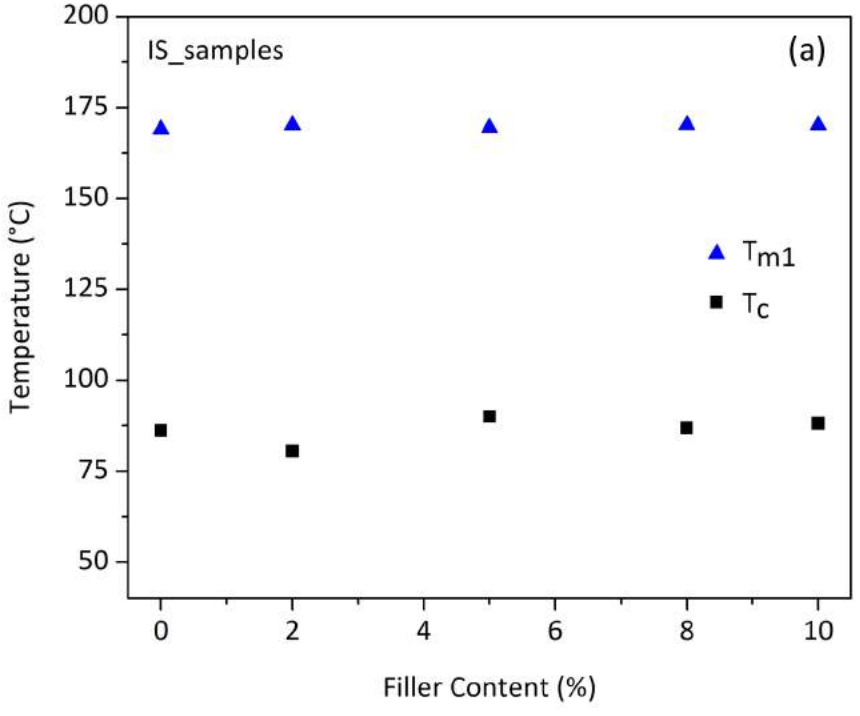
IS_samples
(a)
Temperature (°C)
Filler Content (%)
T_{m1}
T_c
200
175
150
125
100
75
50
0
2
4
6
8
10

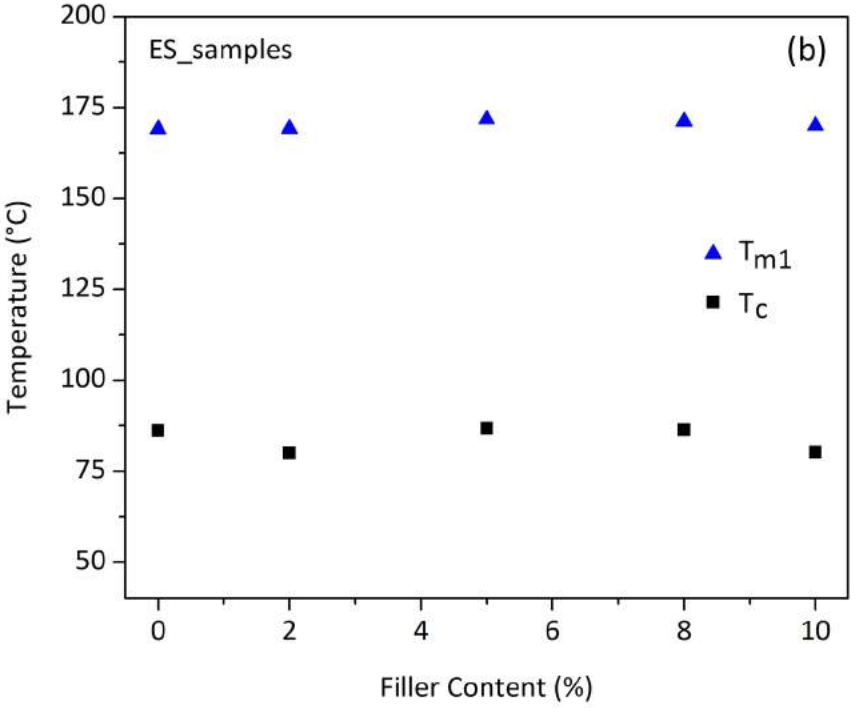
ES_samples
(b)
Temperature (°C)
Filler Content (%)
T_{m1}
T_c
200
175
150
125
100
75
50
0
2
4
6
8
10

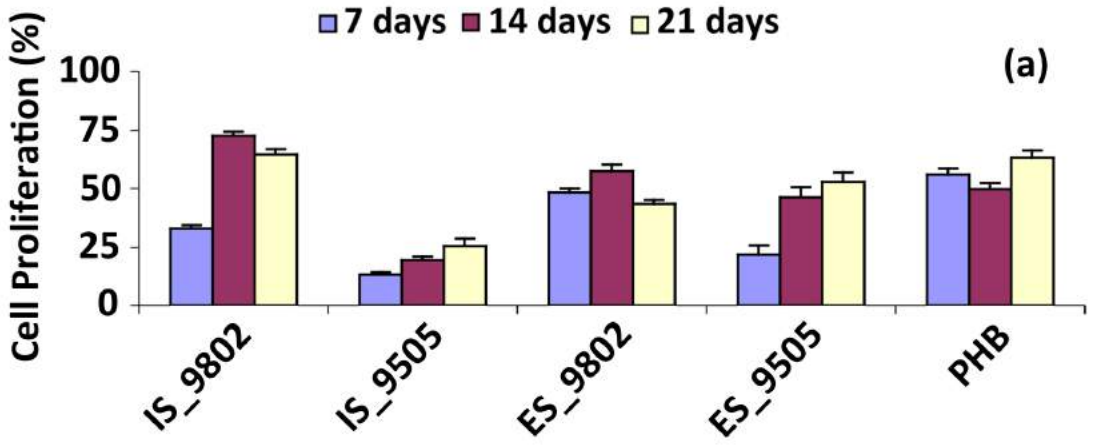
7 days
14 days
21 days
(a)
Cell Proliferation (%)
100
75
50
25
0
IS_9802
IS_9505
ES_9802
ES_9505
PHB

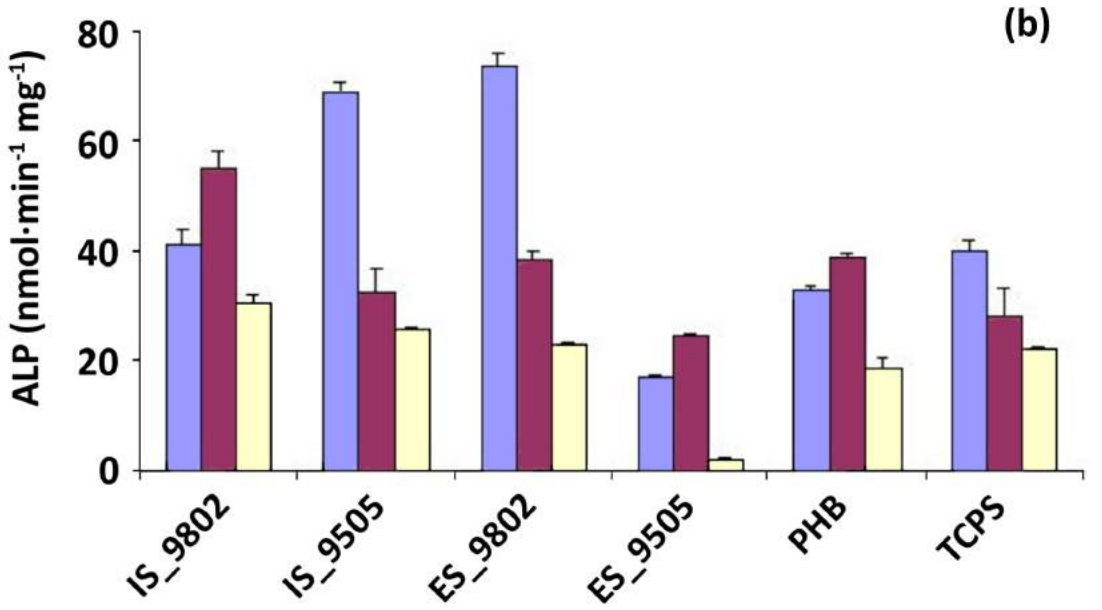
(b)
ALP (nmol·min-1 mg-1)
80
60
40
20
0
IS_9802
IS_9505
ES_9802
ES_9505
PHB
TCPS

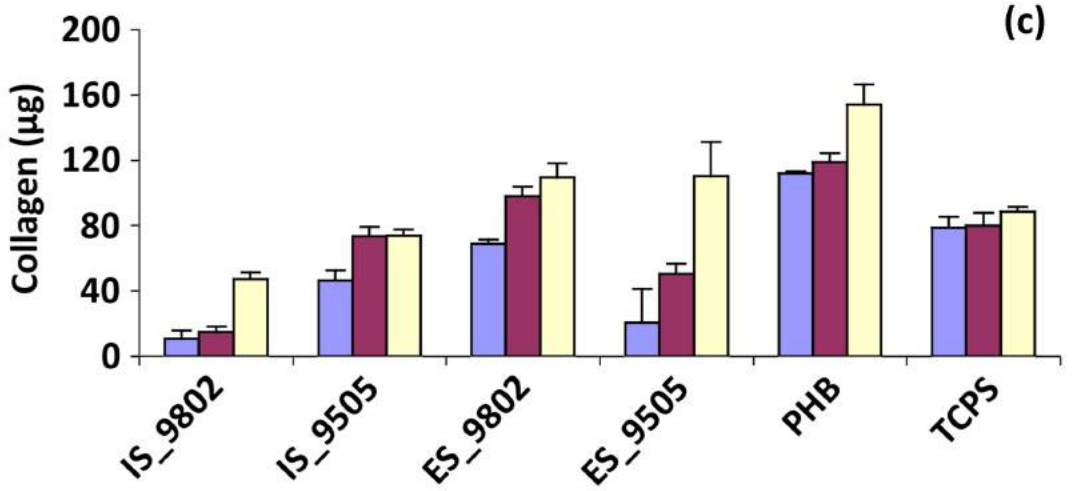
(c)
Collagen (µg)
200
160
120
80
40
0
IS_9802
IS_9505
ES_9802
ES_9505
PHB
TCPS

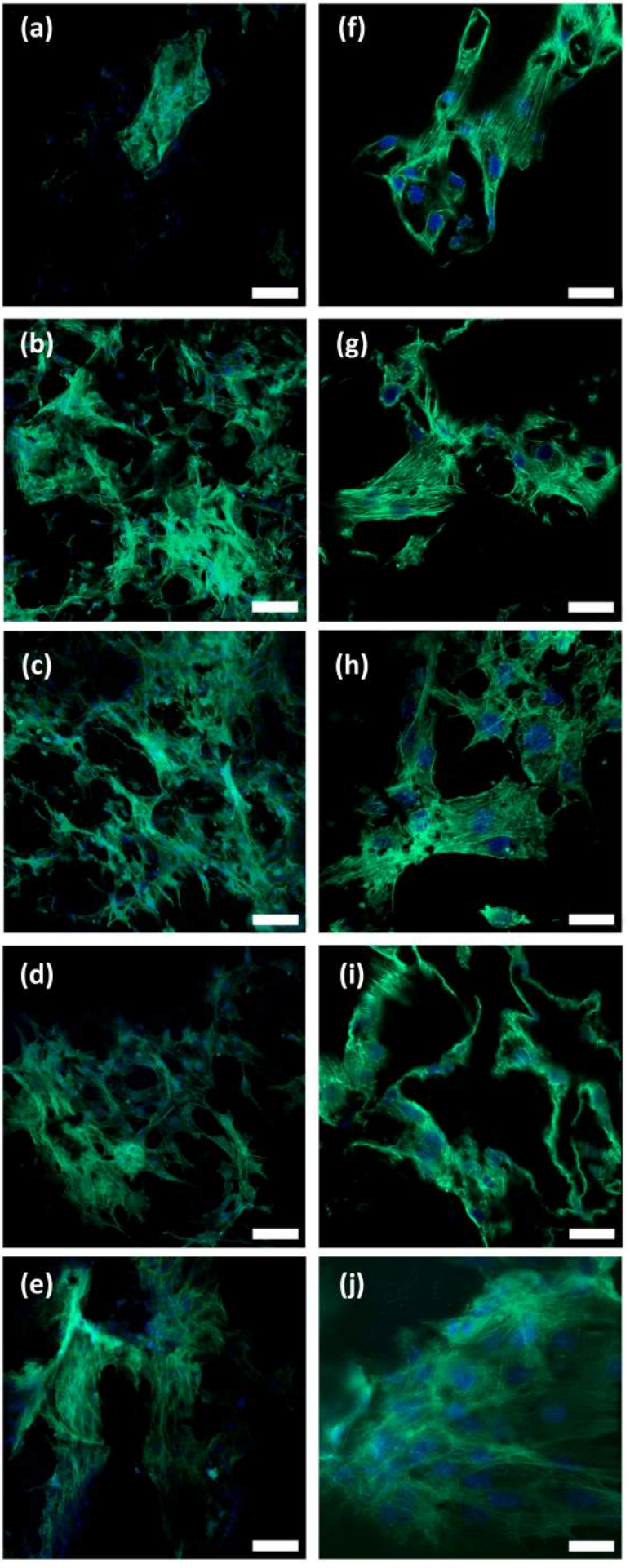
(a)
(f)
(b)
(g)
(c)
(h)
(d)
(i)
(e)
(j)

SUPPORTING INFORMATION

Highly porous PHB-based bioactive scaffolds for bone tissue engineering by *in situ* synthesis of hydroxyapatite

Micaela Degli Esposti [a,b,*], Federica Chiellini [c,b], Federica Bondioli [d,b], Davide Morselli [a,e,*], Paola Fabbri [a,b]

[a] *Department of Civil, Chemical, Environmental and Materials Engineering, Università di Bologna, Via Terracini 28, 40131 Bologna, Italy*

[b] *Consorzio Interuniversitario di Scienza e Tecnologia dei Materiali (INSTM), Via Giusti 9, 50121 Firenze, Italy*

[c] *BIOLab Research Group, Department of Chemistry and Industrial Chemistry, Università di Pisa, via Moruzzi 13, 56124 Pisa, Italy*

[d] *Department of Applied Science and Technology, Politecnico di Torino, Corso Duca degli Abruzzi 24, 10129 Torino, Italy*

[e] *Smart Materials, Istituto Italiano di Tecnologia, Via Morego 30, 16163 Genova, Italy*

* Corresponding Authors

Micaela Degli Esposti, micaela.degliesposti@unibo.it

Davide Morselli, davide.morselli6@unibo.it

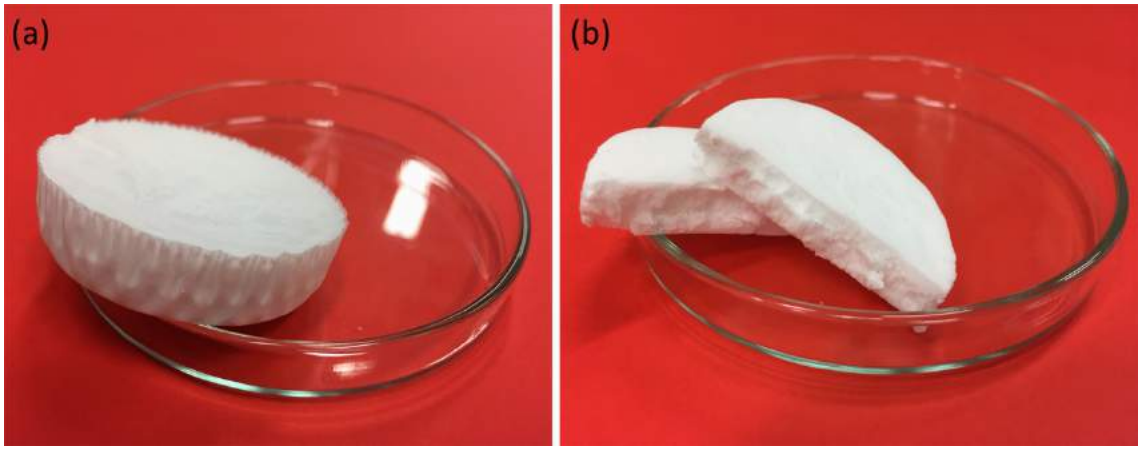

Figure S1. Representative photographs of the (a) whole prepared scaffolds and (b) related cross section.

Table S1. Compressive moduli and related standard deviations for neat PHB and composites scaffolds.

Sample	**Compressive Modulus (KPa)**
PHB	2.58±0.54
ES_9802	4.24±1.93
ES_9505	5.24±2.01
ES_9208	99.5±34.0
ES_9010	3606±1036
IS_9802	5.46±1.79
IS_9505	5.78±1.32
IS_9208	60.5±14.0
IS_9010	1889±110

Crystallites size estimation: the average crystallites size was calculated by the well-known Scherrer equation [*J. Appl. Cryst.* (1978) **11**, 102-113]. The four main peaks at 31.7, 32.2, 32.8 and 35.3 2θ° in the diffractograms of bare HA particles at the bottom of figure 2a and 2b of the manuscript were processed by peaks' fitting and refinement, in order to correctly estimate the average crystallites sizes by the Scherrer equation. Moreover, the contribution due to the instrumental broadening was previously evaluated collecting the diffraction patter of Lanthanum hexaboride (NIST SRM 660C LaB6). The final results are the average of the crystallites dimensions calculated from each above-motioned peak.

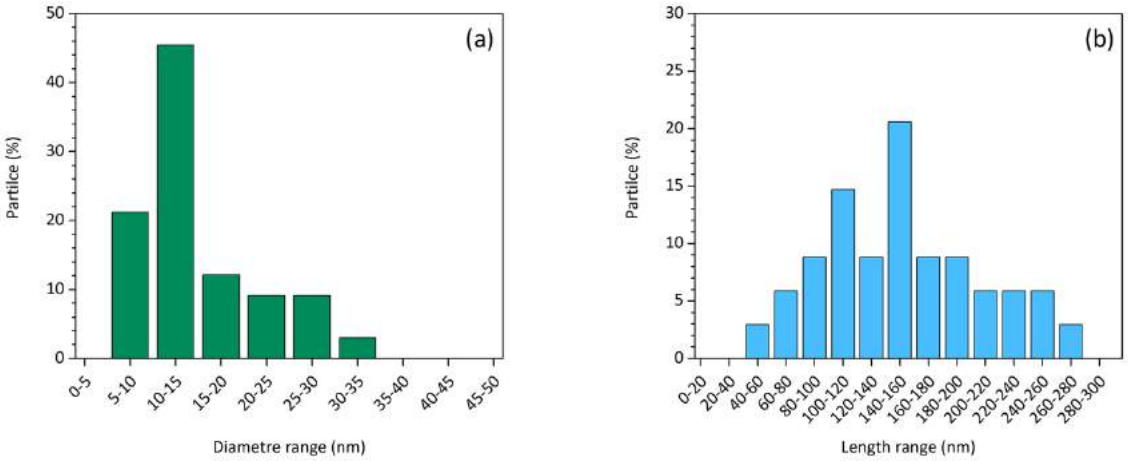

Figure S2. (a) Diametre distribution and (b) length distribution of the HA particles.

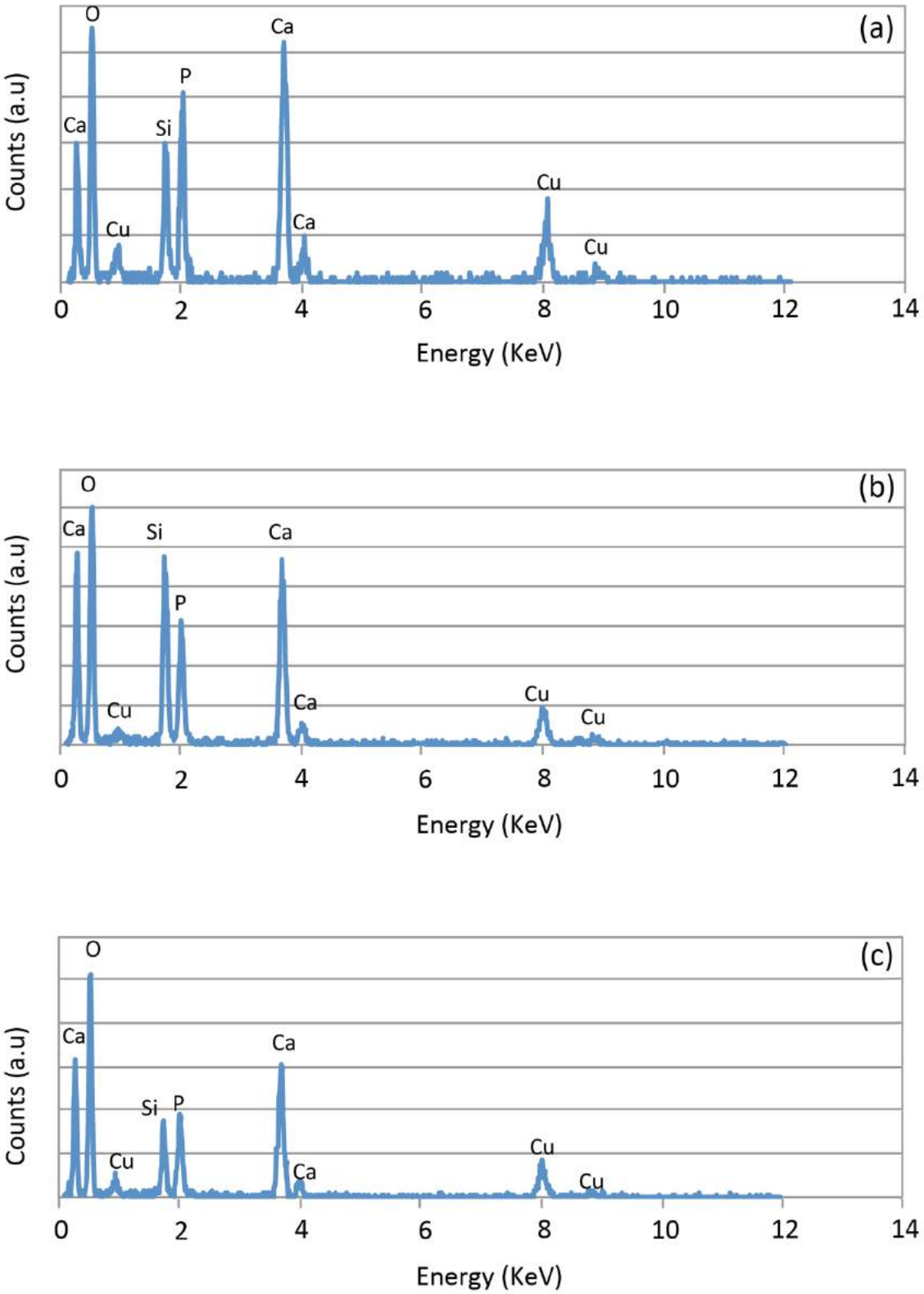

Figure S3. Energy-dispersive X-ray (EDS) analysis performed on the HA particles shown in (a) Figure 2c, (b) Figure 2d and (c) Figure 2e reported in the main manuscript.

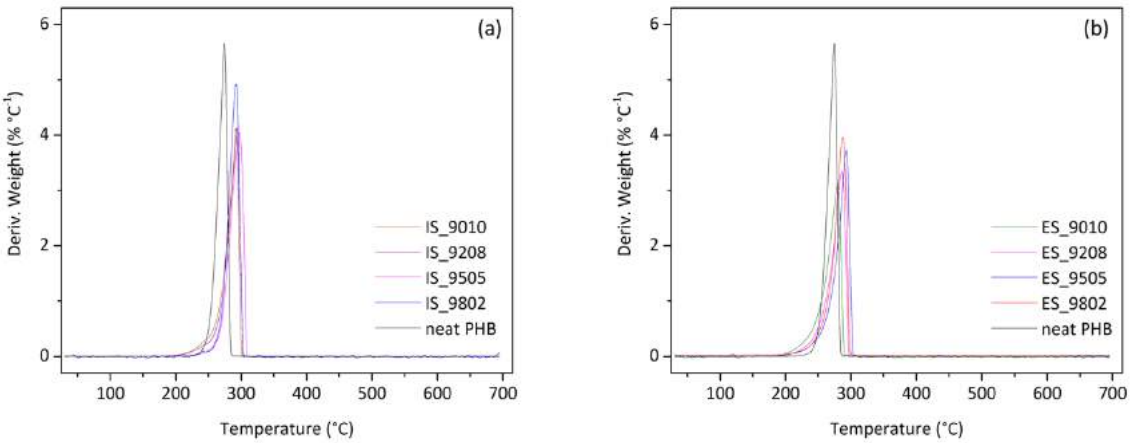

Figure S4. Derivative weight loss curves of the TGA tests in Figure 2a and 2b in the main manuscript. Samples prepared by (a) *in situ* and (b) *ex situ* approach.

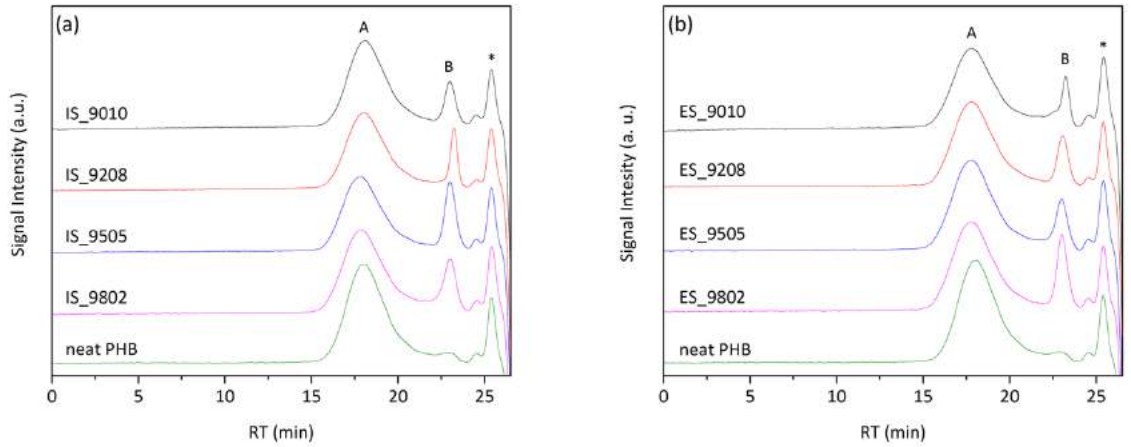

Figure S5. Chromatograms of the samples prepared by (a) *in situ* and (b) *ex situ* approach. A, B and asterisks (*) indicate peak A (higher molecular weight), peak B (lower molecular weight) and toluene peak (internal standard), respectively. RT indicates retention/elution time.

Table S2. Polydispersity as determined by gel permeation chromatography for peak A and B and related A/B ratio of the signal intensities.

		Peak A	**Peak B**
Sample	**A/B ratio**	**Polydispersity***	**Polydispersity***
Experimental grade PHB	1.4	3.18	1.14
Purified PHB	24.0	3.70	1.00
PHB	10.1	2.80	1.14
ES_9802	1.2	3.17	1.00
ES_9505	1.8	2.94	1.14
ES_9208	1.7	3.28	1.00
ES_9010	1.6	2.62	1.00
IS_9802	1.6	2.57	1.00
IS_9505	1.1	2.66	1.00
IS_9208	1.3	2.85	1.00
IS_9010	2.0	2.77	1.14

(*) Polydispersity as M_w/M_n

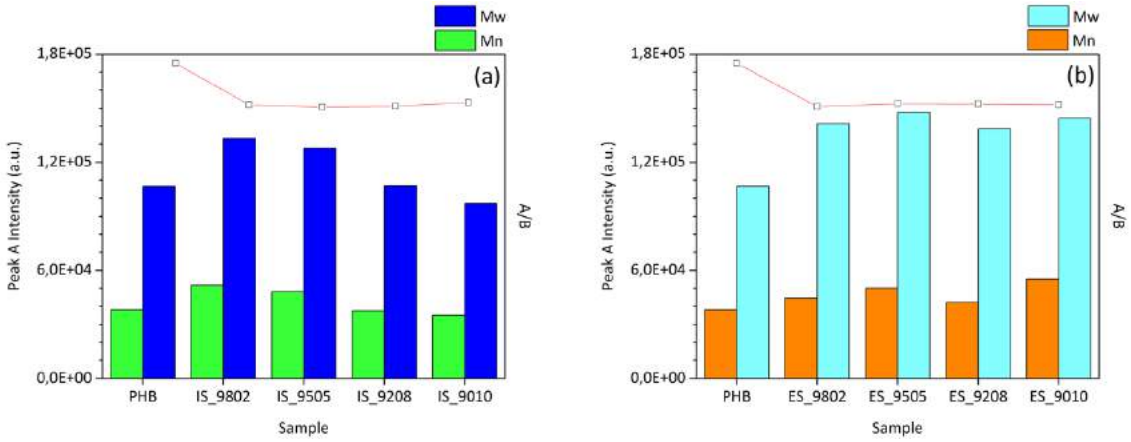

Figure S6. Average molecular weight (M_w), number average molecular weight (M_n) and A/B ratio (□ and red solid line) for samples prepared by (a) *in situ* and (b) *ex situ* approach.

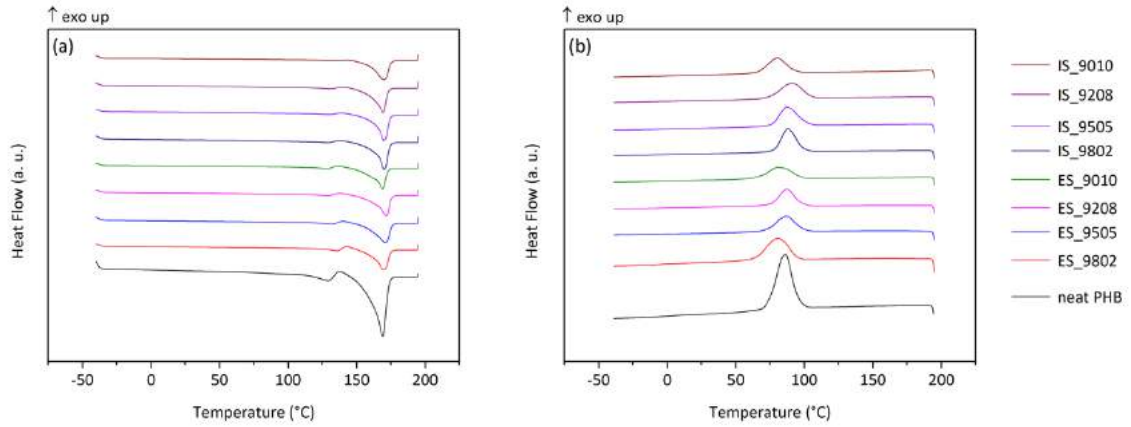

Figure S7. DSC thermograms of all prepared samples obtained from the first (a) heating and (b) cooling cycle.

Table S3. Open porosity (P_0) calculated by Equation 1 for the scaffold used for biological tests.

Sample	**P_0 (%)**
ES_9802	92.0±1.9
ES_9505	90.8±0.8
IS_9802	95.4±0.6
IS_9505	94.2±1.3